JHEP

Published for SISSA by Springer

Received: December 2, 2014
Accepted: January 14, 2015
Published: February 3, 2015

Prospects for dark matter searches in the pMSSM

Leszek Roszkowski,[1] **Enrico Maria Sessolo and Andrew J. Williams**

National Centre for Nuclear Research,
Hoża 69, 00-681 Warsaw, Poland

E-mail: L.Roszkowski@sheffield.ac.uk,
Enrico-Maria.Sessolo@fuw.edu.pl, Andrew.Williams@fuw.edu.pl

Abstract: We investigate the prospects for detection of neutralino dark matter in the 19-parameter phenomenological MSSM (pMSSM). We explore very wide ranges of the pMSSM parameters but pay particular attention to the higgsino-like neutralino at the ~ 1 TeV scale, which has been shown to be a well motivated solution in many constrained supersymmetric models, as well as to a wino-dominated solution with the mass in the range of 2–3 TeV. After summarising the present bounds on the parameter space from direct and indirect detection experiments, we focus on prospects for detection of the Cherenkov Telescope Array (CTA). To this end, we derive a realistic assessment of the sensitivity of CTA to photon fluxes from dark matter annihilation by means of a binned likelihood analysis for the Einasto and Navarro-Frenk-White halo profiles. We use the most up to date instrument response functions and background simulation model provided by the CTA Collaboration. We find that, with 500 hours of observation, under the Einasto profile CTA is bound to exclude at the 95% C.L. almost all of the ~ 1 TeV higgsino region of the pMSSM, effectively closing the window for heavy supersymmetric dark matter in many realistic models. CTA will be able to probe the vast majority of cases corresponding to a spin-independent scattering cross section below the reach of 1-tonne underground detector searches for dark matter, in fact even well below the irreducible neutrino background for direct detection. On the other hand, many points lying beyond the sensitivity of CTA will be within the reach of 1-tonne detectors, and some within collider reach. Altogether, CTA will provide a highly sensitive way of searching for dark matter that will be partially overlapping and partially complementary with 1-tonne detector and collider searches, thus being instrumental to effectively explore the nearly full parameter space of the pMSSM.

Keywords: Supersymmetry Phenomenology

ArXiv ePrint: 1411.5214

[1]On leave of absence from the University of Sheffield, U.K.

doi:10.1007/JHEP02(2015)014

Contents

JHEP02(2015)014

1 Introduction

The search for particles that comprise the dark matter (DM) in the Universe has in recent years made much progress. Alternative and complementary experimental strategies are employed ranging from direct detection of DM-nucleon scattering in underground laboratories, to indirect detection of DM through observation of the Standard Model (SM) products of annihilation in astrophysical phenomena (for a recent review of the large number of experiments dedicated to direct and indirect detection of DM see, e.g., the updated version of [1] in [2] and References therein), to DM direct production at colliders [3, 4].

The most impressive advances in sensitivity have arguably been made in direct detection experiments, where improvement happened rapidly and led to the most recent null results by XENON100 [5] and LUX [6]. As a consequence, the upper bounds on the spin-independent DM-nucleon elastic scattering cross section, $\sigma_p^{\rm SI}$, have become increasingly constraining for many models of weakly interacting massive particles (WIMPs). On the other hand, interesting upper bounds on the cross section for WIMP production [7–10] have been placed at the LHC, which have become particularly constraining for many models of low-mass DM. At the same time, strong limits on the present-day DM annihilation cross section, σv, as a function of the WIMP mass, have been provided by γ-ray experiments. In particular, the most stringent ones for masses up to $\sim 1\,$TeV come from Fermi-LAT's data on dwarf Spheroidal Galaxies (dSphs) [11]. For larger masses the air Cherenkov radiation telescope H.E.S.S. produces the strongest limits from observation of the Galactic Center (GC) [12]. The strongest indirect limits on the spin-dependent DM-proton cross section, $\sigma_p^{\rm SD}$, have instead been obtained at IceCube/DeepCore [13, 14] and ANTARES [15] in

observations of neutrinos from the Sun, and in monojet searches at the LHC [9] for some choices of interactions and mediator masses.

From a theoretical perspective, the most interesting solution to the DM puzzle arguably still comes from low scale supersymmetry (SUSY), as SUSY has the ability to solve many long-standing theoretical issues within one and the same elegant framework. In common scenarios where the lightest SUSY particle (LSP) is the lightest neutralino of the Minimal Supersymmetric Standard Model (MSSM) and makes up all of the DM in the Universe many of the experiments mentioned above have already started to exclude important parts of the parameter space. Some of the solutions [16–18] previously favoured by considerations of electro-weak (EW) naturalness, featuring the neutralino as a somewhat balanced admixture of higgsino and gaugino quantum states with a mass m_χ in the range 80 to 200 GeV now show significant tension [19, 20] with the limits from XENON100 and LUX. The same mixed solutions also start to show some tension [19] with the limits on $\sigma_p^{\rm SD}$ from IceCube and ANTARES. On the other hand, under the assumption that the lightest chargino and second lightest neutralino are not much heavier than the lightest neutralino, the regions of SUSY parameter space characterised by bino-like neutralinos with mass $m_\chi \lesssim 100 - 300\,\text{GeV}$ (depending on whether light sleptons are present) are starting to be probed [19, 21–24] by EW-ino searches at the LHC [25–28].

At the same time, it has been shown [20, 29–34] in global fits of the Constrained MSSM (CMSSM) [35] and Non-Universal Higgs Model (NUHM) that one of the consequences of the discovery at the LHC of a $\sim 125\,\text{GeV}$ Higgs boson [36, 37] in agreement with the SM is that the now favoured parameter space quite naturally gives rise to DM candidates heavier than previously thought. Typically, the $\sim 1\,\text{TeV}$ almost pure higgsino, whose existence as a solution for DM in the MSSM has been long known [38, 39] but in the framework of unified SUSY was first pointed out in a pre-LHC study of the NUHM [40], is now substantially favoured in the above mentioned CMSSM and NUHM and in some non-universal scenarios characterised by reduced EW fine tuning [41–43]. On the other hand, in "split" SUSY scenarios with anomaly mediation [44, 45], which also rose in popularity [46–49] after the Higgs discovery, the wino is the DM. To be a thermal relic that satisfies the relic density its mass should be even larger, in the range 2–3 TeV.

Incidentally, because of its relatively large cross sections for annihilations to SM particles, the wino LSP features excellent indirect detection prospects, which have been recently investigated in several papers [50–52]. The annihilation cross section is enhanced in this case by inclusion of the Sommerfeld enhancement [53, 54], a nonperturbative effect which affects σv and also modifies the expectations for the relic density [55–57]. It is particularly substantial for the thermal wino, which has now consequently been excluded at the 95% C.L. by the absence of specific signatures in existing γ-ray observatories, particularly a monochromatic line in H.E.S.S. data [58]. (The limit is relaxed [52] if one assumes a flat halo profile, like the Burkert profile [59].)

On the other hand, no such statement can be made for the other TeV-scale DM candidates of the MSSM, like the $\sim 1\,\text{TeV}$ almost pure higgsino for which the Sommerfeld enhancement is much less important. Additionally, TeV-scale neutralinos lie probably outside of the direct reach of the LHC, and existing indirect detection experiments will not

JHEP02(2015)014

reach enough sensivity to test them either. The prospects for direct detection at 1-tonne detectors are, on the other hand, very good [19, 20] but upon hypothetical direct detection of a 1 TeV higgsino complementary detection by some other means will be necessary to specify its properties.

Such complementarity will likely be provided by the Cherenkov Telescope Array (CTA) [60]. The CTA project will build the next generation air Cherenkov telescope observatory. Several sensitivity studies [61–64] have shown that for DM masses greater than $\sim 100\,\mathrm{GeV}$ CTA is expected to significantly exceed current limits for WIMP annihilation from the Cherenkov imaging telescopes H.E.S.S. [65], MAGIC [66], and VERITAS [67], and those from Fermi-LAT [11]. CTA may even probe cross sections below the "canonical" thermal relic value of $2.6 \times 10^{-26}\,\mathrm{cm}^3/\mathrm{s}$ for some final states.

In a previous study [20] we showed that CTA has the potential to probe the $\sim 1\,\mathrm{TeV}$ higgsino region of the CMSSM and NUHM parameter space. As mentioned above, this is the region that our Bayesian analysis found to be favoured by the constraints in those models, encompassing approximately 70% of the 2σ credible region in the CMSSM and 90% of it in the NUHM. In this paper we extend the study of direct and indirect DM detection prospects to the more general 19 dimensional low-scale parametrisation called p19MSSM, or more commonly pMSSM [68]. The reason for this is twofold: on the one hand, free gaugino mass terms will allow us to cover a greater number of possibilities for heavy SUSY DM: nearly pure higgsinos, winos, and bino/higgsino/wino admixtures; on the other hand, by additionally floating the scalar soft terms we try to fully incorporate the effects of the most common mechanisms of coannihilation with the lightest neutralino, and of mass degeneracies in general, on the calculation of the relic density. As will be made clear in section 3, these effects can lead to substantial extensions of the allowed parameter space.

In this paper we will pay particular attention to neutralinos around the TeV scale, which seem to be favoured after the discovery of the Higgs boson, and to the sensitivity of CTA, which is naturally poised to probe that particular region of the parameter space. We also review the present status of direct and indirect detection constraints on the pMSSM and compare the reach of CTA with that of 1-tonne direct detection experiments and of other detection methods.

The sensitivity of CTA to the pMSSM and its complementarity to other DM searches has also been recently analysed in ref. [69]. Some of the conclusions of this paper overlap with that study, but we also present several elements not included in [69]:

- We use the most up to date [70] instrument response functions and background estimates provided by the CTA Collaboration [71].

- The sensitivity of CTA is calculated from a binned likelihood function defined on the signal and background regions, similarly to what was done in ref. [64]. (The details of our calculation are presented at the end of this paper, in appendix A.)

- We present results for CTA sensitivity under both the Einasto [72] and Navarro-Frenk-White (NFW) [73] DM halo profiles.

JHEP02(2015)014

- Our analysis takes into account the Sommerfeld enhancement and the consequent limits on wino DM.

The paper is organised as follows: in section 2 we specify the parameter and prior ranges of our scans and their distributions. We present there the set of experimental constraints applied to the likelihood. In section 3 we describe the DM properties of the parameter space regions favoured by the experimental constraints, the dominant annihilation mechanisms, and we identify a few benchmark points for future detection of DM. In section 4 we present a summary of the present status of direct and indirect bounds on neutralino DM and we expose future prospects for detection, particularly at CTA, for which we accurately calculate the sensitivity reach; we also present a comparison with present and future complementary experiments. We finally give our conclusions in section 5. The details of our calculation of CTA's sensitivity including a treatment of alternative statistical approaches are given in appendix A.

2 Scanning methodology and experimental constraints

The pMSSM with 19 free parameters gives a generic coverage of the properties of the CP and R parity conserving MSSM. The parameters are defined at the scale of the geometrical average of the physical stop masses, $M_{\rm SUSY} = (m_{\tilde{t}_1} m_{\tilde{t}_2})^{1/2}$, and we scan them in the ranges given in table 1. In addition, we scan over the top quark pole mass, M_t, treated here as a nuisance parameter. We assume a Gaussian distribution for M_t, whose central value and experimental error are given in [74], $M_t = 173.34 \pm 0.76\,\text{GeV}$. The remaining SM nuisance parameters are fixed to their PDG [2] central values as their variation is less relevant in our study.

For scanning we use the package BayesFITS [19, 31, 75, 76], which interfaces several publicly available tools to direct the scanning procedure and calculate physical observables. The sampling is performed by `MultiNest` [77] with 20,000 live points. The evidence tolerance is set to 0.0001 so that the stopping criterion is not reached before we collect a number of points deemed adequate for our purposes. We use `SoftSusy` v.3.3.9 [78] to calculate the mass spectrum. Higher-order corrections to the Higgs mass are calculated with `FeynHiggs` v.2.10.0 [79–83]. `FeynHiggs` is interfaced with `HiggsSignals` [84] and `HiggsBounds` [85–87] to evaluate the constraints on the Higgs sector. `SuperISO` v.3.3 [88] is used to calculate BR $\left(\overline{\rm B} \to {\rm X_s}\gamma\right)$, BR $\left({\rm B_s} \to \mu^+\mu^-\right)$, BR $\left({\rm B_u} \to \tau\nu\right)$, and $\delta\left(g-2\right)_\mu$. M_W, $\sin^2\theta_{\rm eff}$, ΔM_{B_s} are calculated using `FeynHiggs`. Dark matter observables $\Omega_\chi h^2$, $\sigma_p^{\rm SI}$, $\sigma_p^{\rm SD}$, and σv, the annihilation branching ratios, the photon fluxes for CTA and Fermi-LAT, the neutrino-induced muon flux for IceCube, and the positron flux are computed using `micrOMEGAs` v.3.5.5 [89].

The scans are subject to a set of constraints, applied through a global likelihood function $\mathcal{L}$. The list of constraints, central values, theoretical and experimental uncertainties are presented in table 2. We assume Gaussian distributions for the constraints, with the exception of those on the Higgs sector, which are imposed through `HiggsSignals` and `HiggsBounds`, and the constraints on $\sigma_p^{\rm SI}$ from LUX [6]. The LUX bound, which slightly

JHEP02(2015)014

Parameter	Range
Higgsino/Higgs mass parameter	$-10 \leq \mu \leq 10$
Bino soft mass	$-10 \leq M_1 \leq 10$
Wino soft mass	$0.1 \leq M_2 \leq 10$
Gluino soft mass *	$-10 \leq M_3 \leq 10$
Top trilinear soft coupl.	$-10 \leq A_t \leq 10$
Bottom trilinear soft coupl.	$-10 \leq A_b \leq 10$
τ trilinear soft coupl.	$-10 \leq A_\tau \leq 10$
Pseudoscalar physical mass	$0.1 \leq m_A \leq 10$
1st/2nd gen. soft L-slepton mass	$0.1 \leq m_{\tilde{L}_1} \leq 10$
1st/2nd gen. soft R-slepton mass	$0.1 \leq m_{\tilde{e}_R} \leq 10$
3rd gen. soft L-slepton mass	$0.1 \leq m_{\tilde{L}_3} \leq 10$
3rd gen. soft R-slepton mass	$0.1 \leq m_{\tilde{\tau}_R} \leq 10$
1st/2nd gen. soft L-squark mass	$0.75 \leq m_{\tilde{Q}_1} \leq 10$
1st/2nd gen. soft R-squark up mass	$0.75 \leq m_{\tilde{u}_R} \leq 10$
1st/2nd gen. soft R-squark down mass	$0.75 \leq m_{\tilde{d}_R} \leq 10$
3rd gen. soft L-squark mass	$0.1 \leq m_{\tilde{Q}_3} \leq 10$
3rd gen. soft R-squark up mass	$0.1 \leq m_{\tilde{t}_R} \leq 10$
3rd gen. soft R-squark down mass	$0.1 \leq m_{\tilde{b}_R} \leq 10$
ratio of Higgs doublet VEVs	$1 \leq \tan\beta \leq 62$

Table 1. Prior ranges for the pMSSM parameters, over which we perform our scans. All masses and trilinear couplings are given in TeV.

* In order to avoid generating a large number of points strongly disfavoured by the LHC we impose an additional cutoff on the physical gluino mass, $m_{\tilde{g}} \geq 0.75$ TeV.

improved on the limit from XENON100 [5], is included in the likelihood function following the procedure described in detail in [19, 20, 42, 90]. Additionally, we impose 95% C.L. lower bounds from direct searches at LEP [2], smeared with 5% theoretical errors. The limits are given in eq. (2) of ref. [19], with the exception of the limit on the neutralino mass that has been replaced here by the LEP limit on the invisible Z width, $\Gamma(Z \to \chi\chi)$ [2]. The points are gathered through several scans with both linear and log priors for the mass parameters.

We do not directly impose bounds on sparticle masses from direct SUSY searches at the LHC. As was explained in section 1 we are particularly interested here on neutralino masses predominantly in the range of a few hundred GeV to a few TeV, which are outside the reach of the LHC. The implementation of LHC searches in the likelihood function is for the pMSSM a numerically intensive task [19, 97] that goes beyond our purpose here. We will explicitly mention in the text any situation in which a potential conflict with the limits from the LHC arises.

JHEP02(2015)014

Constraint	Mean	Exp. Error	Th. Error	Ref.
Higgs sector	See text.	See text.	See text.	[84–87]
LUX	See [20, 42].	See [20, 42].	See [20, 42].	[6]
$\Omega_\chi h^2$	0.1199	0.0027	10%	[91]
$\sin^2\theta_{\rm eff}$	0.23155	0.00015	0.00015	[92]
$\mathrm{BR}\left(\overline{\mathrm{B}} \to \mathrm{X_s}\gamma\right) \times 10^4$	3.43	0.22	0.21	[93]
$\mathrm{BR}\left(\mathrm{B_u} \to \tau\nu\right) \times 10^4$	0.72	0.27	0.38	[94]
ΔM_{B_s}	17.719 ps^{-1}	0.043 ps^{-1}	2.400 ps^{-1}	[92]
M_W	80.385 GeV	0.015 GeV	0.015 GeV	[92]
$\mathrm{BR}\left(\mathrm{B_s} \to \mu^+\mu^-\right) \times 10^9$	2.9	0.7	10%	[95, 96]
$\Gamma(Z \to \chi\chi)$	≤ 1.7 MeV	0.3	—	[2]

Table 2. The experimental constraints applied in this study.

Although some of the scans are also driven by the constraint on the anomalous magnetic moment of the muon, $\delta\left(g-2\right)_\mu$ [98, 99], we present our results irrespective of whether the measurement of $\delta\left(g-2\right)_\mu$ is satisfied, as the result is still somewhat controversial and favours the low-mass neutralino region, which is starting to show some tension with data from the LHC.

When appropriate, we present results for two cases. In the first, $\Omega_\chi h^2 \simeq 0.12$, we consider a Gaussian distribution for the relic density of DM, with experimental and theoretical uncertainties added in quadrature. In the second case, $\Omega_\chi h^2 \lesssim 0.12$, the relic density is imposed as an upper bound only, by means of a half Gaussian likelihood.

3 Neutralino properties and benchmark points

In this and the following sections we show in the plots only the points the satisfy the constraints of table 2 at the 95% C.L., i.e., we select $\Delta\chi^2 \leq 5.99$ from the current best-fit point, where $\chi^2 = -2\ln(\mathcal{L}/\mathcal{L}_{\rm max})$.

In figure 1(a) we show the distribution of our scan points in the $(m_\chi,\, \sigma v)$ plane for the case where the LSP saturates the relic abundance, $\Omega_\chi h^2 \simeq 0.12$. We remind the reader that $\sigma v = \langle\sigma v\rangle|_{p\to 0}$. The colour code gives the composition of the lightest neutralino. The equivalent distribution in the $(m_\chi,\, \sigma_p^{\rm SI})$ plane is shown in figure 1(b). The LUX bound on $\sigma_p^{\rm SI}$ is included in the likelihood; as a consequence in figure 1(b) almost no points lie above the 90% C.L. limit, shown here with a dashed red line for clarity.

As is well known, the neutralino mass and composition are determined by the relic density because it is a strong constraint with a relatively small uncertainty. The points of the elongated, almost vertical branches at $m_\chi < 100$ GeV belong to the Z- and h-resonance "regions" [100]. The neutralino mass is approximately half the mass of the Z boson or of the lightest Higgs, so that resonant annihilation in the early Universe leads to the correct relic density. The neutralino is predominantly bino-like with a small admixture of higgsino

JHEP02(2015)014

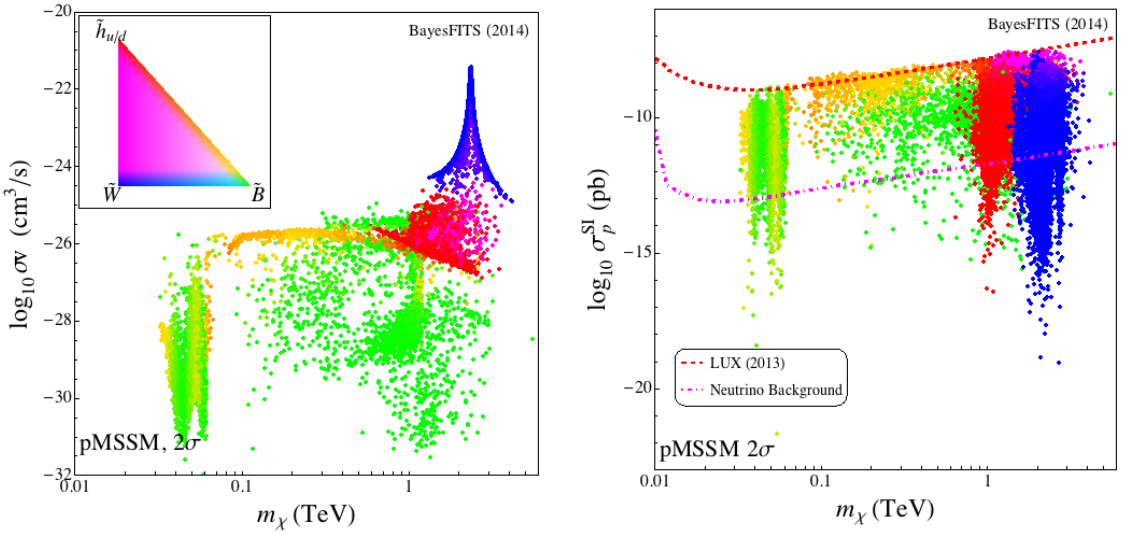

(a) **(b)**

Figure 1. (a) The distribution of the points with $\Delta\chi^2 \leq 5.99$ (see table 2) in the (m_χ, σv) plane. The colour coding identifies the composition of the lightest neutralino. Pure states are shown in green for the bino ($\tilde{B}$), blue for the wino ($\tilde{W}$), and red for the higgsino ($\tilde{h}_{u/d}$). Admixtures are shown with intermediate colours in accordance with the legend. (b) Same as (a) but in the (m_χ, $\sigma_p^{\rm SI}$) plane. The dashed red line shows the 90% C.L. bound from LUX [6], included in the likelihood. The dot-dashed magenta line shows the onset of the irreducible atmospheric and diffuse supernova neutrino background [101–103].

that does not exceed $\sim 40\%$. Because of their relatively low mass, neutralinos in this region will be the first among the SUSY particles to be tested at the LHC 14 TeV run, possibly even through direct DM production as in the monojet/monophoton searches, which provide limits that do not depend on the presence of light charginos or sleptons in the spectrum. On the other hand, because of their suppressed present-day annihilation cross section these points are in principle not very interesting for indirect detection.

As the neutralino mass increases, $m_\chi > 100\,\text{GeV}$, predominantly bino-like LSPs (in green) satisfy the relic density through different well-understood mechanisms. From the left to the right, the point models are characterised by "bulk-like" annihilation to leptons [104, 105], slepton/neutralino co-annihilation [106], or resonance with heavy A/H Higgs bosons [105].[1]

In the range $0.1\,\text{TeV} \lesssim m_\chi \lesssim 1\,\text{TeV}$, neutralinos characterised by a mixed bino/higgsino composition satisfy the relic abundance partially through annihilation to gauge bosons, but also through off-shell Z exchange into top quarks, which can become dominant above the threshold since the other fermionic final states are suppressed by helicity conservation. The WIMPs in this region generally feature a large spin-independent cross section, so that if they have not been excluded by XENON100/LUX they are situated

[1] A more detailed description of the mass ranges associated with each mechanism in a 9-dimensional low-scale parametrisation of the MSSM (p9MSSM) can be found in [19].

JHEP02(2015)014

just below the 90% C.L. bound in figure 1(b). Some of the points surviving the bound show significant higgsino levels but a relative sign difference between μ and M_1 suppresses the coupling of the neutralino to the lightest Higgs boson. Additionally, cancellations between the heavy and light Higgs diagrams reduce $\sigma_p^{\rm SI}$ giving rise to known "blind spots" [107–111]. The position and depth of these spots depend on the relative sign of μ and M_1 and generally require that the masses of the heavy Higgs bosons are not much above the TeV scale.

Note also that in the pMSSM there exists the additional possibility of augmenting neutralino annihilations in the early Universe with co-annihilations with a squark or gluino. This allows combinations of higgsino and bino components that can effectively evade the direct detection experiments. One can see some examples of this in the mixed points at $m_\chi \gtrsim 1\,\text{TeV}$. For indirect detection this scenario can feature a relatively large annihilation cross section but if co-annihilations are the dominant mechanism then this can be reduced below the projected sensitivity of CTA.

For masses equal and slightly larger than 1 TeV, almost pure higgsinos naturally satisfy the relic density and direct detection constraints simultaneously. Figure 1(a) shows that for these points (in red) the present-day annihilation cross section is large enough to be of interest to CTA. Pure higgsinos can lead to the correct relic density by quite a diversified set of annihilation mechanisms in the early Universe. Annihilation to gauge/Higgs bosons and chargino co-annihilation are the most natural options for masses on and above 1 TeV, but one can see in figure 1(a) some other higgsino points at 2–2.5 TeV, for which the above-mentioned coannihilations with stops or gluinos effectively decrease the relic abundance. Conversely, for lower mass higgsinos, with m_χ as small as $\sim 600\,\text{GeV}$, mass degeneracies with sleptons and squarks increase the number of degrees of freedom at freeze-out, thus effectively boosting the value of the relic density with respect to the case without degeneracy [112]. Additionally, one can see a large set of higgsino points above the "canonical" thermal relic value for the cross section. There, σv is enhanced by a large resonant effect with the heavy Higgs bosons A/H that was thermally washed out in the early Universe (for an explanation see, e.g., appendix B of ref. [19]).

An almost pure wino LSP (in blue) can naturally satisfy the relic density for masses around 2.8–3 TeV [57]. As was the case for the nearly pure higgsino, winos can have masses that extend over a much larger interval, $1.6\,\text{TeV} \lesssim m_\chi \lesssim 4\,\text{TeV}$ thanks to coannihilations with squarks and gluinos, which reduce the relic density, or mass degeneracies with lighter scalar particles, which can increase it.

One can see in figure 1(a) that Early Universe annihilation and co-annihilation of the winos receive a boost from the Sommerfeld enhancement [55–57]. We incorporated this effect as a correction factor to $\Omega_\chi h^2$, which we extrapolated from figure 5 of ref. [57] and from ref. [56]. We also modified the present-day annihilation cross section by the rescaling factors derived for different final states in [113] for the case of wino DM. We smeared the rescaling factors with a quadratic function of $\Delta m_\chi = m_{\chi_1^\pm} - m_\chi$ to extend the Sommerfeld effect to the few mixed wino/higgsino points featured in our scan. The effects of the Sommerfeld enhancement can be seen in the peculiar "Eiffel Tower" shaped resonance in figure 1(a) for wino (in blue) and mixed wino/higgsino LSPs (in magenta).

JHEP02(2015)014

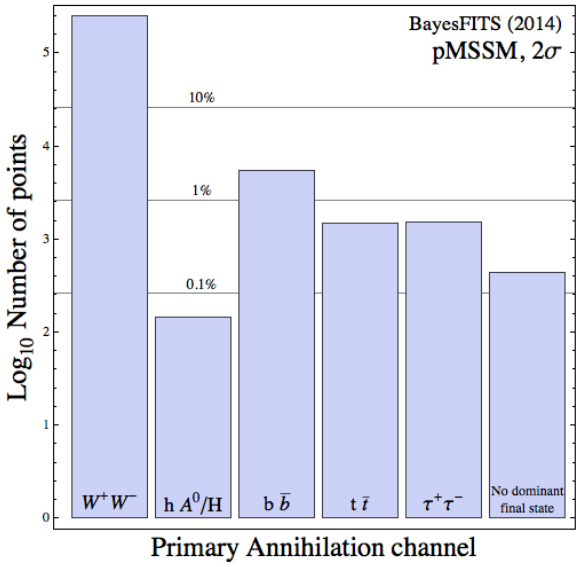

Figure 2. Bar chart of the points in the scan ($\Delta\chi^2 \leq 5.99$) according to their primary annihilation channel (the primary final state is the one with the largest branching fraction).

Additionally, the spectrum also features an enhanced $\chi\chi \to \gamma\gamma$ cross section. Because of this, scenarios dominated by wino DM are in conflict with data from the current generation of γ-ray telescopes, namely they are excluded [50–52] at the 95% C.L. by the H.E.S.S. search for γ-ray lines [58], with the exception of cases where the halo profile is very flat. We will show in section 4.1 that the same result applies to the wino-like points in our scans.

The bar chart in figure 2 shows the number of points with $\Delta\chi^2 \leq 5.99$ organised by their predominant annihilation channel. We classify each point in terms of which final state has the largest branching fraction but for the majority of points annihilation will occur to several different final states. One can see that the largest number predominantly annihilates into W^+W^-, which is the preferred final state for both the higgsino and wino high-density regions in figure 1.

In figure 3(a) we show the distribution in the $(m_\chi, \sigma v)$ plane of the points in the first column of figure 2 (largest branching ratio to W^+W^-). The colour code shows the actual value of the branching ratio for each point. The distributions of the points in the 3rd ($b\bar{b}$), 4th ($t\bar{t}$), and 5th ($\tau^+\tau^-$) columns of figure 2 are shown in figures 3(b), 3(c), and 3(d), respectively. To allow a direct comparison, in the panels of figure 3 we indicate with a dashed black line the expected reach of CTA in the relative final state. We will discuss in detail in section 4.2 and appendix A the sensitivity of CTA. In figure 3 we also mark with orange stars the positions of a few benchmark points for indirect detection, which we present in table 3 and whose characteristics we describe below.

In figure 3(a) one can see that the ~ 1 TeV higgsino region must feature very substantial branching fractions to subdominant final states other than W^+W^-. In general, higgsinos can often have an almost equal branching fraction to ZZ, Zh or ZA, through t-channel exchange of the neutral, almost degenerate second-lightest neutralino. In figure 3(b) one can see that points annihilating into $b\bar{b}$ final states are very common and spread over the

JHEP02(2015)014

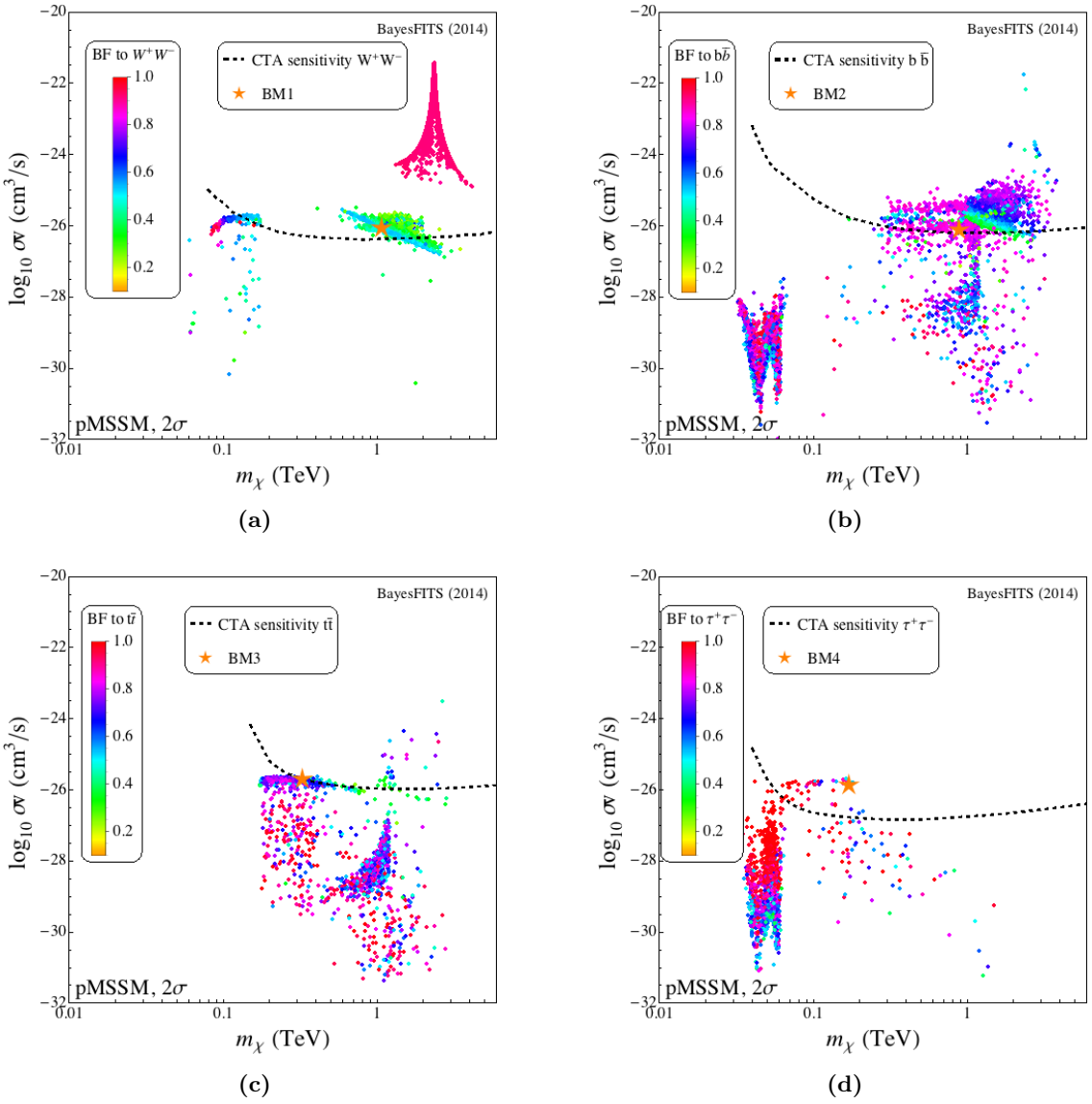

Figure 3. (a) Distribution in the (m_χ, σv) plane of the points with $\Delta\chi^2 \leq 5.99$ (see table 2) annihilating primarily into W^+W^-. The colour code shows the value of the W^+W^- branching fraction for each point. The dashed black line shows the projected sensitivity of CTA to points with BR($\chi\chi \to W^+W^-$) = 100%, which we derive in appendix A. The orange star marks the position of BM1. (b) Same as (a) but for $b\bar{b}$. The orange star marks the position of BM2. (c) Same as (a) but for $t\bar{t}$. The orange star marks the position of BM3. (d) Same as (a) but for $\tau^+\tau^-$. The orange star marks the position of BM4.

JHEP02(2015)014

Benchmark	BM1	BM2	BM3	BM4
M_1	Decoupled	878	353	-189
M_2	Decoupled	Decoupled	1500	Decoupled
μ	-1057	1300	-369	218
m_A	Decoupled	1832	2500	754
$\tan\beta$	58.0	49.4	26.6	30.0
$m_{\tilde{\tau}_R}$	Decoupled	Decoupled	Decoupled	253
m_χ	1077	883	328	172
Composition	$\lvert N_{\tilde{B}}\rvert^2 = 0.000015$ $\lvert N_{\tilde{W}}\rvert^2 = 0.000076$ $\lvert N_{\tilde{h}_u}\rvert^2 = 0.5$ $\lvert N_{\tilde{h}_d}\rvert^2 = 0.5$	$\lvert N_{\tilde{B}}\rvert^2 = 0.996$ $\lvert N_{\tilde{W}}\rvert^2 = 4\times10^{-7}$ $\lvert N_{\tilde{h}_u}\rvert^2 = 0.00313$ $\lvert N_{\tilde{h}_d}\rvert^2 = 0.00136$	$\lvert N_{\tilde{B}}\rvert^2 = 0.730$ $\lvert N_{\tilde{W}}\rvert^2 = 0.00043$ $\lvert N_{\tilde{h}_u}\rvert^2 = 0.156$ $\lvert N_{\tilde{h}_d}\rvert^2 = 0.114$	$\lvert N_{\tilde{B}}\rvert^2 = 0.777$ $\lvert N_{\tilde{W}}\rvert^2 = 0.00084$ $\lvert N_{\tilde{h}_u}\rvert^2 = 0.142$ $\lvert N_{\tilde{h}_d}\rvert^2 = 0.080$
$\Omega_\chi h^2$	0.119	0.121	0.119	0.122
Main mechanism $\Omega_\chi h^2$	chargino co-ann. $\chi\chi^\pm \to$ SM	A-resonance $\chi\chi \to b\bar{b}$	s ch. off-shell Z $\chi\chi \to t\bar{t}$	t-ch. exch. $\tilde{\tau}$,$\chi_1^\pm$,$\tilde{\chi}_2^0$ $\chi\chi \to \tau^+\tau^-$, $W^+W^-, t\bar{t}, ZZ$
σv (cm^3/s)	8.45×10^{-27}	7.59×10^{-27}	1.96×10^{-26}	1.34×10^{-26}
Branching fractions	53.8% W^+W^- 45.1% ZZ 0.983% $t\bar{t}$ 0.116% Zh	79.7% $b\bar{b}$ 20.2% $\tau^+\tau^-$ 0.1% $d\bar{d}/s\bar{s}$	74.1% $t\bar{t}$ 12.9% W^+W^- 10.4% ZZ 1.9% Zh	36.4% $\tau^+\tau^-$ 31.1% W^+W^- 24.5% ZZ 7.2% $b\bar{b}$
$\sigma_{\gamma\gamma}v$ (cm^3/s)	5.31×10^{-29}	1.04×10^{-33}	2.32×10^{-30}	1.58×10^{-30}
$\sigma_{Z\gamma}v$ (cm^3/s)	4.75×10^{-29}	3.04×10^{-34}	1.86×10^{-29}	1.11×10^{-29}
$\sigma_p^{\rm SI}$ (pb)	4.73×10^{-12}	1.65×10^{-10}	3.37×10^{-9}	1.14×10^{-9}
$\sigma_p^{\rm SD}$ (pb)	7.75×10^{-9}	1.17×10^{-7}	7.51×10^{-5}	1.55×10^{-4}

Table 3. Benchmark points for indirect detection. SUSY masses are given in GeV. "Decoupled" stands for any mass value above 5000 GeV.

entire range of the parameter space. These are typical of the A-resonance mechanism, when $m_A \approx 2m_\chi$, and they are characterised by moderate-to-large $\tan\beta$. Note that, for $\tan\beta \lesssim 8$, points characterised by resonance with the heavy Higgses prefer to annihilate to $t\bar{t}$ instead. One can see these points in figure 3(c) for masses $m_\chi \gtrsim 500$ GeV (in the same part of the figure many points are also characterised by stop co-annihilation in the early Universe). The points at $m_\chi < 500$ GeV in figure 3(c) are instead points that satisfy the relic density through selectron (or smuon) co-annihilation, or annihilation to tops through an off-shell Z, for which s-wave production of light fermions is helicity-suppressed.

JHEP02(2015)014

In figure 3(d) one can see that many of the points that satisfy the relic density at the Z/h-resonance, $m_\chi \simeq 45 - 65\,\text{GeV}$, very predominantly annihilate in the present-day Universe to $\tau^+\tau^-$ and their cross section is depleted with respect to the "canonical" thermal value. This is because, on the one hand the Boltzman distribution for WIMPs in this range is sharply peaked at momentum $p > 0$ so that one expects a drop in the cross section now, when $p \to 0$; on the other hand, the lightest stau happens to be for these points light enough ($m_{\tilde{\tau}_1} \simeq 100-500\,\text{GeV}$) to allow significant annihilation to taus through stau exchange in the t channel. Note that even if the points in this region are predominantly bino-like they need a non-negligible amount of mixing with the higgsino to efficiently annihilate in the early Universe. Thus, for many of these points the lightest chargino, $\chi_1^\pm$, and the second-lightest neutralino, $\tilde{\chi}_2^0$, have masses not much far above m_χ, and they are therefore very likely to be already excluded by 3-lepton searches at the LHC [25–28]. However, there are several other points in this region for which $m_{\chi_1^\pm} \gtrsim 450\,\text{GeV}$ so that they are not currently excluded and remain viable scenarios. The 14 TeV run at the LHC should definitively probe these points.

We present four benchmark points for DM detection in table 3, each one is marked by an orange star in the panels of figure 3. They are chosen such that they are not presently excluded but represent scenarios within the projected reach of CTA.

Benchmark point 1 (BM1) belongs to the $\sim 1\,\text{TeV}$ higgsino region. The dominant final states are W^+W^- and ZZ. The $\gamma\gamma$ and $Z\gamma$ cross sections are suppressed compared to the continuous spectrum but remain relatively large due to the higgsino nature of the neutralino and the associated light chargino that appears in the loops. Benchmark point 2 (BM2) is a typical A-resonance point annihilating predominately to $b\bar{b}$. It is the only benchmark point without sizeable higgsino-bino mixing. Due to this the $\gamma\gamma$ and $Z\gamma$ cross sections are heavily suppressed. Benchmark point 3 (BM3) is a mixed bino-higgsino neutralino. The $t\bar{t}$ final state is produced non-resonantly and thus requires large mixing to increase the coupling of the neutralino to the Z boson. The chargino associated with the higgsino component is relatively light and induces the sub-dominant annihilation channels to W^+W^- and ZZ. Finally, benchmark point 4 (BM4) is another mixed bino-higgsino neturalino similar to BM3 although its dominant annihilation channel is now mediated by a light stau leading to a $\tau^+\tau^-$ final state. For BM4 the neutralinos in the early Universe also annihilate into top quarks at threshold, but top production is suppressed for $p \to 0$ because the neutralino is slightly too light.

It should be noted that both mixed bino-higgsino scenarios, BM3 and BM4, have a spin-independent scattering cross section close to the current limit from LUX, thus making these scenarios highly visible in future direct detection experiments. BM2 may be detectable at future 1-tonne direct detection experiments, while BM1 lies in a direct detection blind spot.

4 Prospects for dark matter detection

We present here the prospects for DM detection in the pMSSM. In section 4.1 we summarise the current status of indirect-detection bounds on the parameter space of the pMSSM. We show the case where the neutralino saturates the relic abundance, $\Omega_\chi h^2 \simeq 0.12$, and the case $\Omega_\chi h^2 \lesssim 0.12$. In section 4.2 we present our estimate of the sensitivity reach of CTA.

JHEP02(2015)014

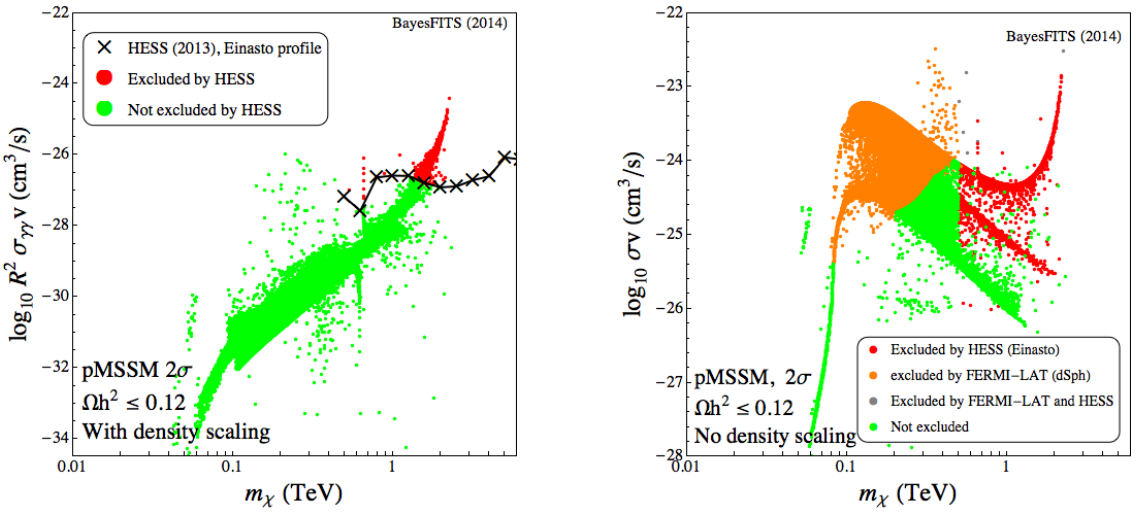

Figure 4. Current status of indirect detection bounds on the pMSSM for $\Omega_\chi h^2 \lesssim 0.12$. (a) The points excluded at the 95% C.L. by γ-ray line searches at H.E.S.S. [58] (in red) in the (m_χ, $R^2 \cdot \sigma_{\gamma\gamma} v$) plane. (b) The points excluded at the 95% C.L. by Fermi-LAT dSphs [11] (orange) and H.E.S.S. γ-ray line search (red) in the (m_χ, σv) plane (case without rescaling).

We give results for the Einasto and NFW DM halo profiles, obtained through the procedure described in detail in appendix A. Finally, in section 4.3 we compare the reach of CTA with the sensitivity of other direct and indirect detection experiments.

4.1 Current indirect detection bounds on the pMSSM

It was shown, e.g., in ref. [19] for the p9MSSM and in ref. [69] for the p19MSSM that the bounds from the continuous γ-ray spectrum from dSphs at Fermi-LAT [11] are too weak to affect the MSSM parameter space when the PLANCK value [91] on $\Omega_\chi h^2$ is imposed. The limits can however become important in scenarios where the relic abundance is satisfied as an upper bound only. This opens up large regions of the parameter space, characterised by lighter higgsino and wino LSPs that annihilate away effectively in the early Universe and have a much suppressed relic abundance. These solutions could correspond to a scenario with two-component DM, in which case the sensitivity of Fermi-LAT should be rescaled according to the square of the density, R^2, to account for the reduced present-day density of neutralinos ($R = \Omega_\chi / \Omega_{\rm Planck}$). Alternatively, one can assume that the neutralino represents the entirety of the DM and the correct abundance is fixed by invoking some additional mechanism, e.g., freeze-in [114]. In this case one obtains much stronger limits from indirect detection than in the previous scenario because rescaling by R^2 is not necessary [115]. Only in this case does the limit from dSphs have significant impact on the parameter space. However, the limit from the γ-ray line search at H.E.S.S. [58] can also affect a small part of the parameter space when one applies rescaling.

JHEP02(2015)014

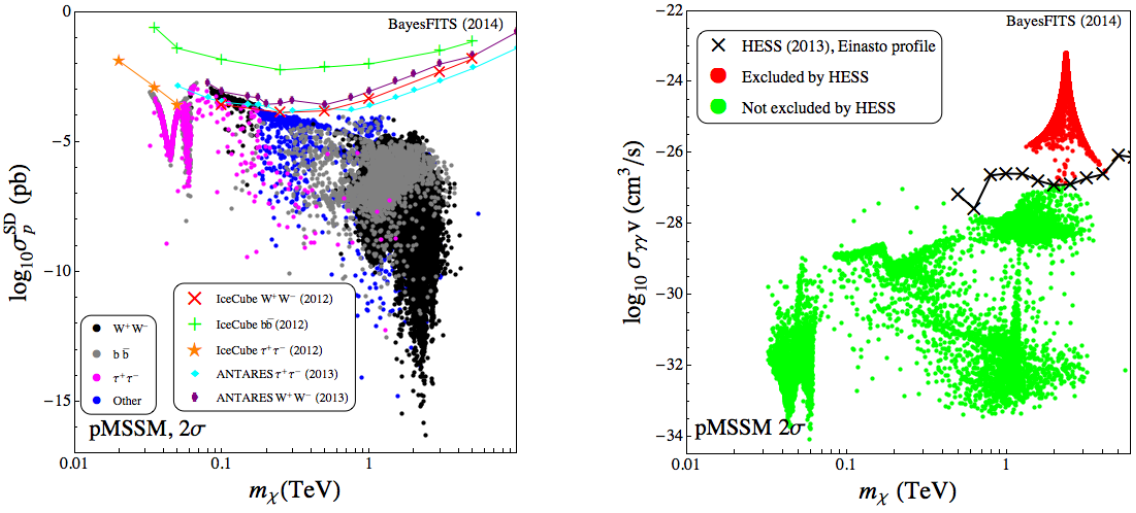

Figure 5. (a) The current 90% C.L. limits on $\sigma_p^{\rm SD}$ from IceCube [13, 14] and ANTARES [15]. The limits are presented for the W^+W^-, $b\bar{b}$, and $\tau^+\tau^-$ final states. Points are shown with $\Delta\chi^2 \leq 5.99$ (see table 2). The colour code shows the primary annihilation final state for each point. (b) The current 95% C.L. limits on $\sigma_{\gamma\gamma}v$ from H.E.S.S. [58]. In red we show the points that are excluded by the experimental bound, indicated with a solid black line. Points are shown with $\Delta\chi^2 \leq 5.99$ (see table 2).

In figure 4(a) we show in red the points excluded at the 95% C.L. by the H.E.S.S. search under the assumption of rescaling by R^2. In figure 4(b) we show the points excluded at the 95% C.L. by Fermi-LAT dSphs (in orange) and the above mentioned H.E.S.S. γ-ray line search (in red) projected to the $(m_\chi, \sigma v)$ plane in the case of no rescaling. In the absence of additional guidance from theory, the real limit is likely to lie somewhere in between the exclusions of figures 4(a) and 4(b).

Going back to the case where the neutralino saturates the relic density, the strongest indirect limits on the spin-dependent scattering cross section come from IceCube/DeepCore [13, 14] and ANTARES [15], from observation of neutrinos from the Sun. It is well known [116] that $\sigma_p^{\rm SD}$ can easily be measured through the relation between the DM solar capture rate and the annihilation rate, which should give rise to a high-energy neutrino spectrum and flux.

In figure 5(a) we show the current limits from IceCube and ANTARES, provided for 100% branching ratios to W^+W^-, $b\bar{b}$, and $\tau^+\tau^-$, compared to the points of the pMSSM. The colour code shows the dominant annihilation final state for each point, in the sense of figure 2.

As was mentioned in section 3 the γ-ray line search at H.E.S.S. [58] is very effective in placing a strong bound on wino DM when $\Omega_\chi h^2 \simeq 0.12$. We show in figure 5(b) the current limit on the cross section under the assumption of the Einasto halo profile, compared to the pMSSM points. As was previously shown in [50–52], when one includes the Sommerfeld enhancement H.E.S.S. excludes at the 95% C.L. pure or almost pure wino DM, with the

JHEP02(2015)014

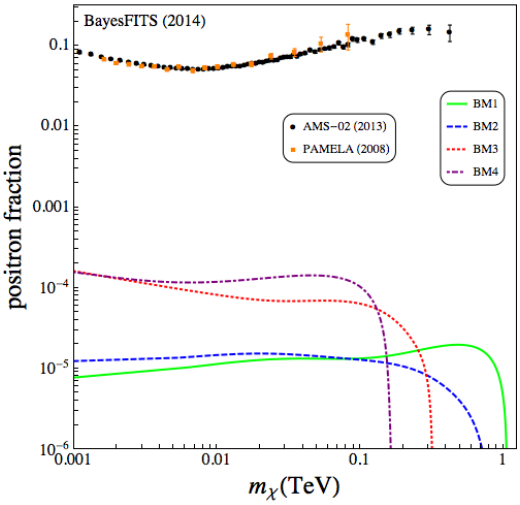

Figure 6. The DM annihilation contribution to the positron fraction for the benchmark points of table 3 compared to the measured positron fraction at Pamela [117] and AMS-02 [118].

exception of cases where a flat DM profile is assumed. (We repeat that we include the Sommerfeld enhancement as a smeared correction factor derived from ref. [113].) Note that it has been recently shown [119] that the estimate of the wino annihilation cross section is subject to a significant perturbative uncertainty. However, even when accounting for these uncertainties the H.E.S.S. limit is still quite constraining for this scenario. For the remainder of this paper we will not show in the plots the points excluded by H.E.S.S..

In figure 6 we show the DM annihilation contribution to the positron fraction for the benchmark points of table 3. We compare our benchmark points to the measured positron fraction at Pamela [117] and AMS-02 [118]. We use `micrOMEGAs` to calculate the produced positron spectrum for each point and the positron flux at the Earth after propagation. We use the default values in `micrOMEGAs` for charged particle propagation. To compare with the positron fraction we use the parametrisation of the primary electron background and secondary electron and positron fluxes following [120, 121]. The fluxes in GeV cm^{-2} s^{-1} sr^{-1} are given by,

$$\left(\frac{d\Phi}{dE}\right)_{\text{primary},\,e^-} = \frac{0.16E^{-1.1}}{1+11E^{0.9}+3.2E^{2.15}}\,, \tag{4.1}$$

$$\left(\frac{d\Phi}{dE}\right)_{\text{secondary},\,e^-} = \frac{0.7E^{0.7}}{1+110E^{2.9}+600E^{2.9}+580E^{4.2}}\,, \tag{4.2}$$

$$\left(\frac{d\Phi}{dE}\right)_{\text{secondary},\,e^+} = \frac{4.5E^{0.7}}{1+650E^{2.3}+1500E^{4.2}+580E^{4.2}}\,. \tag{4.3}$$

For all of the benchmarks the positron flux is many orders of magnitude too small to explain the anomalous positron fraction, which is also true for the rest of the points.

JHEP02(2015)014

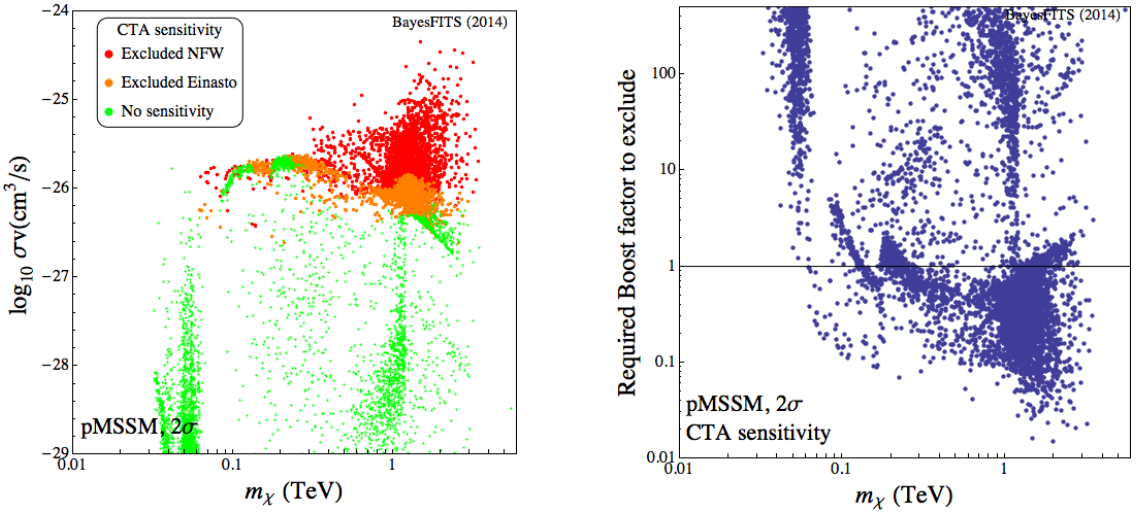

Figure 7. (a) Sensitivity of CTA to the pMSSM in the (m_χ, σv) plane. Red points are within reach of CTA assuming an NFW profile, orange points assuming an Einasto profile, green points are beyond the sensitivity of CTA. Points are shown with $\Delta\chi^2 \leq 5.99$ (see table 2). The details of the calculation are given in appendix A. (b) The boost factor to σv, required for each point to be within the 95% C.L. sensitivity of CTA for the Einasto profile.

4.2 Sensitivity of CTA to the pMSSM

The sensitivity of CTA is obtained by testing the background-only hypotesis with a likelihood function. The construction of the likelihood is detailed in appendix A. We use the most up to date [70] instrument response functions and background estimates provided by the CTA Collaboration [71]. We assume an observation time of approximately 500 hours, and we provide results under the Einasto and NFW DM halo profiles, for which we calculate the J-factors.

We start with the case where the lightest neutralino makes up all of the DM, $\Omega_\chi h^2 \simeq 0.12$. In figure 7(a) we show the 95% C.L. sensitivity of CTA in the (m_χ, σv) plane. We show points within the reach of CTA under the assumption of the NFW profile in red, while the points excluded under the Einasto profile but not the NFW are shown in orange. Green points lie beyond the reach of CTA for either profile. We repeat that we do not show in the plots the points excluded by H.E.S.S. (see figure 5(b)), which feature a nearly pure wino LSP or an admixture of wino and higgsino. Our improved analysis shows that the reach of CTA for SUSY is even more optimistic than our previous study had anticipated [20] and under the Einasto profile CTA is bound to exclude at the 2σ level the ~ 1 TeV higgsino region of the pMSSM in almost its entirety, effectively closing the window for heavy SUSY DM in many realistic models.

The point is emphasised in figure 7(b), where we show the boost factor, b_F, required for each point to be within the 95% C.L. sensitivity of CTA for the Einasto profile. Points below $b_F = 1$ can be excluded without a boost factor. One can see that, in agreement

JHEP02(2015)014

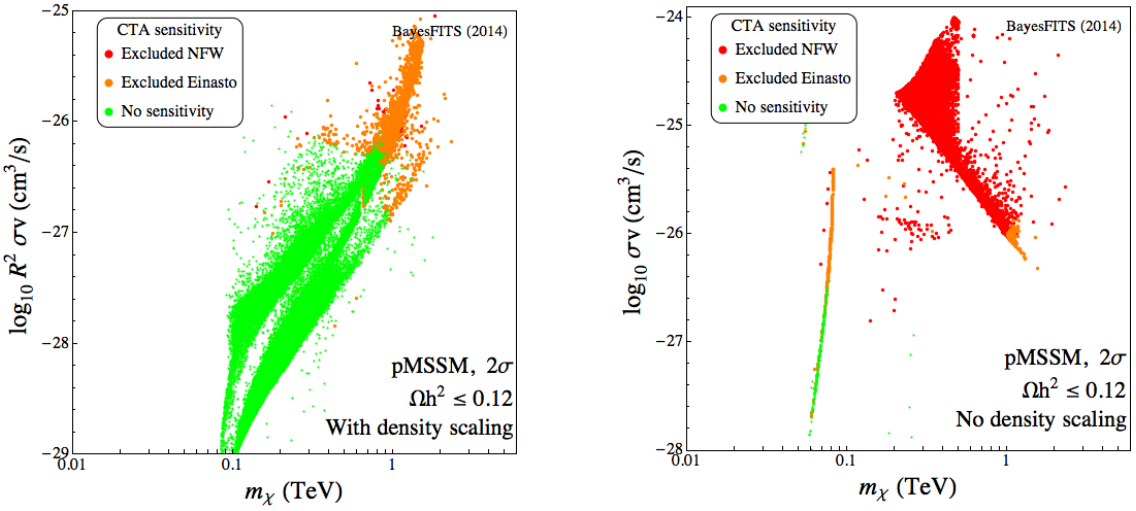

Figure 8. The reach of CTA in the pMSSM for the case $\Omega_\chi h^2 \lesssim 0.12$. The colour code is the same as in figure 7(a). (a) The 95% C.L. reach of CTA in the (m_χ, $R^2 \cdot \sigma v$) plane for the case with rescaling of the local density. (b) The 95% C.L. reach of CTA in the (m_χ, σv) plane for the case without rescaling.

with figure 7(a), the majority of points in the ~ 1 TeV higgsino region do not require any boost factor.

Incidentally, we want to underline here the power of the binned likelihood function especially in relation to the points that show a significant cross section to $\gamma\gamma$. This is what happens for the points in red and orange at $m_\chi < 300$ GeV in figure 7(a), which are projected to be excluded under one or the other profile assumption. Their γ-ray flux effectively gives rise to an excess in one or a few particular bins, large enough to kill the likelihood function irrespectively of all other bins.

It has been suggested in the literature [122, 123] that a better fit for the DM profile in spiral galaxies, including possibly the Milky Way, might be provided by the Burkert rather than the Einasto or NFW profiles. We have checked that the Burkert profile assumption has the effect of weakening the projected reach of CTA in the (m_χ, σv) plane by a factor of ~ 50 with respect to the Einasto profile. Under the Burkert profile assumption figure 7 would have to be modified as follows: on the one hand the ~ 1 TeV higgsino region would be outside of the reach of CTA; on the other hand, the vast majority of the points with wino DM, which are excluded by H.E.S.S. under the Einasto assumption, would then be allowed and directly in reach of CTA.

We now move on to describe the reach of CTA in the case where the neutralino does not saturate the relic density, $\Omega_\chi h^2 \lesssim 0.12$. Figure 8(a) shows the expected reach of CTA in the (m_χ, $R^2 \cdot \sigma v$) plane in the case of rescaling σv by the ratio (squared) of the neutralino density to the PLANCK value. We do not show in the plot the points excluded by Fermi-LAT dSphs and the γ-ray line search at H.E.S.S., see figure 4. One can see that CTA will

JHEP02(2015)014

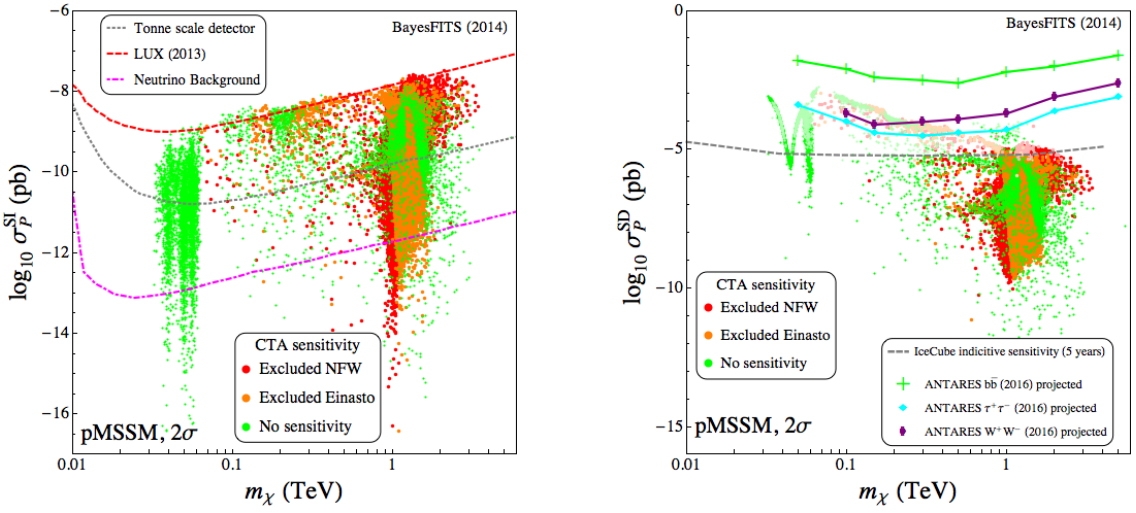

Figure 9. In all panels the colour code is the same as in figure 7(a). Points are shown with $\Delta\chi^2 \leq 5.99$ (see table 2). (a) The sensitivity of CTA to the pMSSM in the $(m_\chi, \sigma_p^{\rm SI})$ plane. The LUX 90% C.L. bound is shown a dashed red line. The projected sensitivity of 1-tonne detectors is shown as a dotted grey line. The onset of the atmospheric and diffuse supernova neutrino background is shown with a dot-dashed magenta line. Note that points are plotted from red to green, showing a conservative estimate of the reach (least constrained points are always shown). (b) The sensitivity of CTA to the pMSSM in the $(m_\chi, \sigma_p^{\rm SD})$ plane. Lighter shaded points are within the projected 5-year sensitivity of IceCube/DeepCore. The dashed grey line is indicative of IceCube's sensitivity. The solid lines show the projected reach at ANTARES [124] for 2016 in the $b\bar{b}$ (green), W^+W^- (purple), and $\tau^+\tau^-$ (cyan) final states.

probe regions of the parameter space beyond the limit presently set by H.E.S.S., especially if one assumes the Einasto halo profile. A few points (in red) are excluded by CTA also under assumption of the NFW profile but in that case much of the parameter space lies beyond the reach of CTA due to the rescaling factor R^2.

As was the case in figure 4, when one assumes no rescaling the sensitivity of CTA can exclude a large fraction of the parameter space under both profile assumptions, as one can see in figure 8(b) where the CTA reach is shown in the $(m_\chi, \sigma v)$ plane.

4.3 Complementarity of CTA with other experiments

In figure 9(a) we show the projected reach of CTA in the $(m_\chi, \sigma_p^{\rm SI})$ plane to compare it with direct detection experiments, which are sensitive to the spin-independent neutralino-proton cross section, $\sigma_p^{\rm SI}$. We use the same colour code as in figure 7(a) for the sensitivity of CTA. The projected sensitivity of XENON-1T [125], indicative of the generic reach of 1-tonne detectors like, e.g., DEAP-3600 [126] and LZ [127], is shown as a dashed grey line. The dot-dashed magenta line shows the onset of the irreducible background due to atmospheric and diffuse supernova neutrinos [101–103]. Since there is considerable overlap between the regions within the reach of CTA and those out of reach, it should be noted that the points

JHEP02(2015)014

are overlaid from the most constrained to the least constrained. Thus, the plots represent a conservative estimate of the reach of CTA in these planes.

Figure 9(a) shows that over most of the pMSSM parameter space the reach of CTA is orthogonal to that of detectors directly measuring $\sigma_p^{\rm SI}$. CTA will be able to probe the vast majority of the points that lie well beyond the reach of 1-tonne detectors and even reach the region where the irreducible neutrino background will strongly curb sensitivity advances for direct detection experiments.

In figure 9(b) we show the sensitivity of CTA compared to the projected 5-year sensitivity of the IceCube/DeepCore 86-string configuration, shown as a light shading in the plot. The sensitivity has been here separately estimated for the IceCube *upward*, IceCube *contained*, and DeepCore contained events, following the procedure described in detail, e.g., in refs. [128, 129]. We take the effective area for IceCube and the effective volume for DeepCore as parametrised in [128, 130, 131]. The light shaded points in figure 9(b) fall within the reach of at least one of these three estimates. The projected 2016 reach in $\sigma_p^{\rm SD}$ at ANTARES [124] in the $b\bar{b}$ (green), W^+W^- (purple), and $\tau^+\tau^-$ (cyan) final states is also shown.

To highlight the idea of complementarity, we show in figure 10(a) the reach of CTA compared to the one of 1-tonne detectors in the ($\sigma_p^{\rm SI}$, σv) plane. The projected sensitivity of CTA appears as horizontal bands that follow the same colour code as in figure 7(a), while the points within the projected reach of 1-tonne detectors are shown as lighter shaded. The dashed grey line vertically separates the points within the sensitivity of 1-tonne detectors (lighter shading) from the ones below sensitivity (regular colouring). In figure 10(b) we present the equivalent picture in the ($\sigma_p^{\rm SD}$, σv) plane, where the light-shaded region indicates the points within 5-year sensitivity at IceCube/DeepCore, and the dashed grey line separates the points within sensitivity from those outside the reach.

As was mentioned in sections 2 and 3, a detailed analysis of the LHC reach in the pMSSM is beyond the scope of this paper because it interests regions of the parameter space characterised by a low mass neutralino, orthogonal in some sense to the regions in which CTA is most sensitive. However, for completeness we show in figure 11 the reach of CTA compared to the present limits on sparticle masses obtained in simplified models at the LHC. These are meant to be seen as a generic indication of the present reach of the LHC and the reader must keep in mind that in complex models a detailed analysis can often produce limits that can be either weaker or stronger than the ones under simplified model assumptions [97].

In figure 11(a) we show the reach of CTA in the ($m_{\tilde{g}}$, m_χ) plane. The solid black line shows the 95% C.L. bound obtained at ATLAS for the simplified model of [132]. The limit obtained at CMS is very similar [135]. The reach of CTA in the ($m_{\tilde{t}_1}$, m_χ), ($m_{\tilde{b}_1}$, m_χ), and ($m_{\chi_1^\pm}$, m_χ) planes is shown in figures 11(b), 11(c), and 11(d), respectively. With the exception of the coannihilation bands, shown in figure 11 as regions of mass degeneracy (e.g. $m_\chi \approx m_{\tilde{g}}$ in figure 11(a)), the reach of CTA is largely independent of the sparticle spectrum, as was to be expected. Improvements in the limits on the gluino and squark masses are not expected to have any effect on the sensitivity of CTA. Indeed, CTA remains sensitive to spectra where the gluinos and squarks lie well beyond the reach of present and future colliders.

JHEP02(2015)014

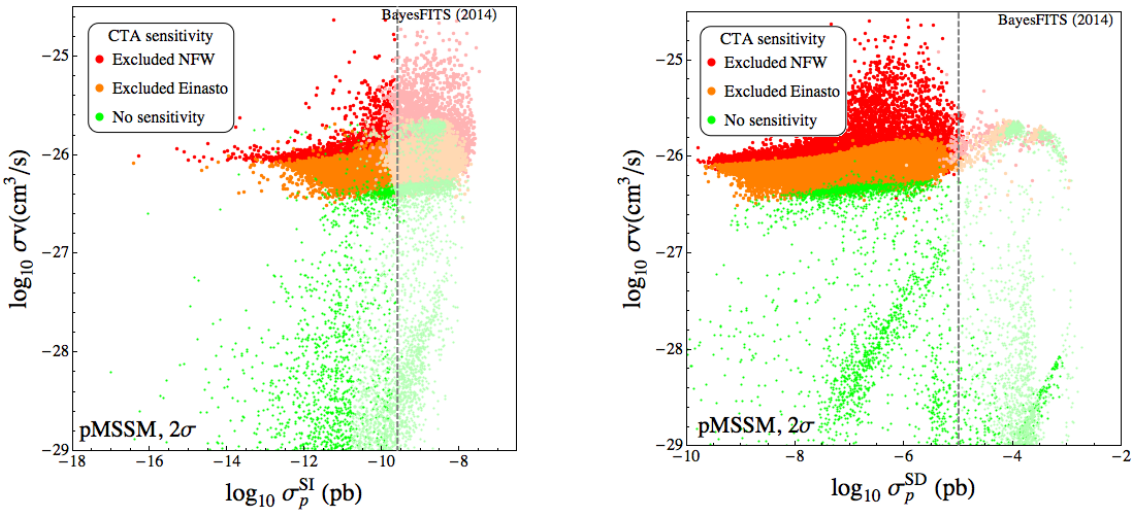

Figure 10. In all panels the colour code is the same as in figure 7(a). Points are shown with $\Delta\chi^2 \leq 5.99$ (see table 2). (a) The sensitivity of CTA to the pMSSM points in the $(\sigma_p^{\rm SI}, \sigma v)$ plane. Lighter shaded points are within the projected sensitivity of 1-tonne detectors. The dashed grey line gives an approximate reference value for future direct detection reach in $\sigma_p^{\rm SI}$. (b) The sensitivity of CTA to the pMSSM points in the $(\sigma_p^{\rm SD}, \sigma v)$ plane. Lighter shaded points are within the projected 5-year sensitivity of IceCube/DeepCore. The dashed grey line gives an approximate reference value for future reach in $\sigma_p^{\rm SD}$.

Note that in figure 11(d) we have indicated with a solid black line the bound from 3 lepton EW-ino searches obtained under the assumption that a light slepton of the first two generations is present and has a mass in between m_χ and $m_{\chi_1^\pm}$ or $m_{\tilde{\chi}_2^0}$ [26, 27]. As it stands the limits seems to exclude almost entirely the Z/h-resonance region of the parameter space, shown in the lower left-hand side of the plot, at $m_\chi < 100\,\text{GeV}$. One must remember that for the points of the pMSSM characterised by heavier sleptons the limit is actually weaker than shown here [26, 28], thus allowing part of the Z/h-resonance region to survive the bounds.

5 Summary and conclusions

In this paper we have investigated the prospects for detection of neutralino DM in the framework of the pMSSM. We have focused here particularly on models for which the LSP is a neutralino at about the TeV scale, outside the reach of the 14 TeV run at LHC. TeV-scale neutralinos have been shown to be promising candidates for DM in many well-motivated SUSY scenarios after the Higgs boson discovery.

In order to satisfy the constraints from the relic density neutralinos in this mass range must preferentially be nearly pure higgsinos, or winos, or a mixture of the two. However, as is known from many studies recently appeared in the literature, thermal-relic winos are subject to large Sommerfeld enhancement of their annihilation cross section, so that they

JHEP02(2015)014

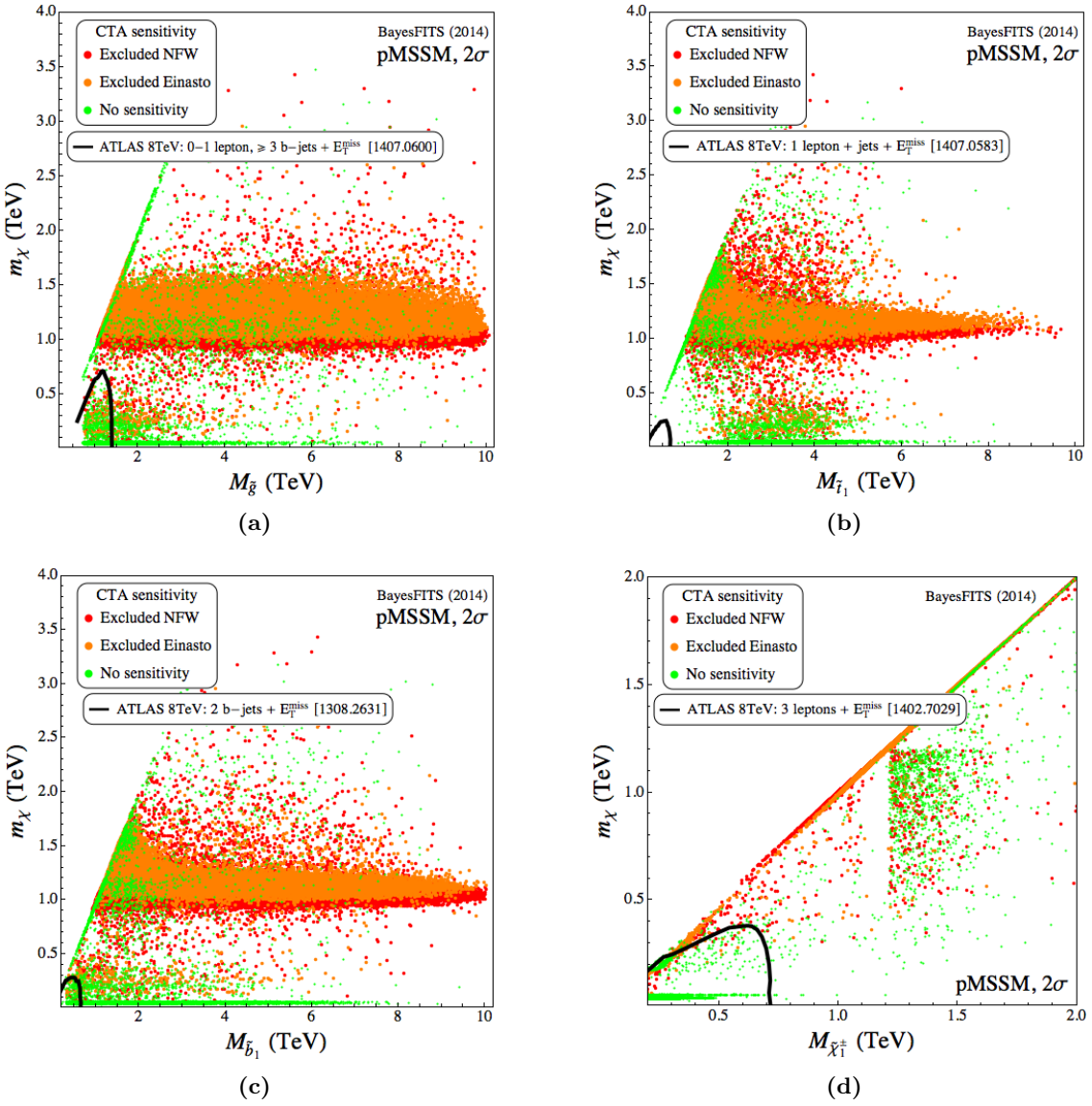

Figure 11. In all panels the colour code is the same as in figure 7(a). (a) Sensitivity of CTA in the $(m_{\tilde{g}}, m_{\chi})$ plane, the thick black line shows the current ATLAS limit in the simplified model of ref. [132]. (b) Sensitivity of CTA in the $(m_{\tilde{t}_1}, m_{\chi})$ plane, the thick black line shows the current ATLAS limit in the simplified model of ref. [133]. (c) Sensitivity of CTA in the $(m_{\tilde{b}_1}, m_{\chi})$ plane, the thick black line shows the current ATLAS limit in the simplified model of ref. [134]. (d) Sensitivity of CTA in the $(m_{\chi_1^{\pm}}, m_{\chi})$ plane, the thick black line shows the current ATLAS limit in the simplified model of ref. [26].

JHEP02(2015)014

are excluded at the 2σ level by the H.E.S.S. search for γ-ray lines from the GC under most choices of the DM halo profile. Consequently the most likely candidate for heavy SUSY DM that is not excluded by the present constraints is the $\sim 1\,\text{TeV}$ nearly pure higgsino.

We showed in this paper that the air Cherenkov radiation telescope array of imminent construction CTA has the sensitivity reach to nearly exclude at the 95% C.L. the $\sim 1\,\text{TeV}$ higgsino region of the pMSSM with 500 hours of observation. We derived the sensitivity of CTA to continuous and γ-ray line photons arising from neutralino DM annihilation by constructing an energy-binned likelihood function and adopted the most up to date estimates of the detector response functions and modelling of the background provided by the CTA Collaboration. We obtained results for the Einasto and NFW profile assumptions. We applied our results to the parameter space of the pMSSM, but also presented the limits for single annihilation final state channels.

We showed that under the NFW profile assumption CTA will be able to probe 70% of the points belonging to the $\sim 1\,\text{TeV}$ higgsino region in our scans, specifically those for which the annihilation cross section is enhanced by one of the following factors: resonance with a heavy Higgs boson, A/H; non-negligible admixture with the wino; or a significant annihilation to a monochromatic $\gamma\gamma$ line. Assumption of the Einasto profile allows us to formulate even more optimistic projections, as we found that in this case CTA will also probe the remaining part of the $\sim 1\,\text{TeV}$ higgsino region, with the exclusion of some points characterised by heavy squark or gluino co-annihilation, and will probe additionally a significant part of the parameter space leading to bino and mixed bino/higgsino DM.

We also found that, in complementarity with other direct and indirect detection experiments, CTA will significantly probe the favoured parameter region of the pMSSM, far beyond the reach of 1-tonne underground detectors alone. We showed that many of the points well within our calculated sensitivity of CTA lie below the onset of the irreducible atmospheric and diffuse supernova neutrino background for direct detection.

Finally we found that by combining different experiments detection prospects for SUSY DM are very good also in scenarios where the neutralino is not the only particle comprising the DM in the Universe. The existing bounds and projections strongly depend in this case on the adopted prescription for rescaling the local DM abundance. We found that even under the most conservative assumption, that the local density is rescaled with the square of the ratio of the neutralino density to the PLANCK value, CTA will be able to exclude a large region of the parameter space, significantly outperforming the reach of current Fermi-LAT dSphs and H.E.S.S. γ-ray line searches.

Acknowledgments

We would like to thank John Carr for useful discussions on the CTA project and for supplying us the latest detector response functions and background simulation. We would also like to thank Vincent Bertin for providing us the projected sensitivity of ANTARES. A.J.W. would like to thank Alexander Pukhov for clarifying some issues regarding `micrOMEGAs`. This work has been funded in part by the Welcome Programme of the Foundation for Polish Science. L.R. is also supported in part by a STFC consortium grant of Lancaster,

JHEP02(2015)014

Manchester, and Sheffield Universities. The use of the CIS computer cluster at the National Centre for Nuclear Research is gratefully acknowledged. L.R. would like to thank the Theory Division of CERN for hospitality during the final stages of the project.

A Derivation of the CTA reach

In this appendix we present the calculation of CTA's sensitivity to the WIMP annihilation cross section. We compare the sensitivities that can be obtained through different likelihood functions, and we refer to some other recent work on the subject that can be found in the literature [61–64].

We use the *Ring Method* as defined in [61–64]. Two regions are identified in the plane of the galactic coordinates l and b, as shown in figure 12. The "signal", or ON, region is based on a circle of angular radius $\Delta_{\rm cut} = 1.36^\circ$ around the GC. The "background", or OFF, region is based on a ring centred at the offset coordinate $b_{\rm off} = 1.42^\circ$, with an inner angular radius of $r_1 = 0.55^\circ$ and an outer radius of $r_2 = 2.88^\circ$, from which the ON region is subtracted. The strip of sky characterised by $|b| < 0.3^\circ$ about the GC and the region of the sky within the inner radius r_1 do not belong to either the ON or OFF regions.

We proceed to create a binned likelihood function. For each energy bin, i, the expected number of counts from DM annihilation is calculated:

$$N_i^{\rm ann} = t_{\rm obs} \cdot J \cdot \frac{\sigma v}{8\pi m_\chi^2} \int_{\Delta E_i} dE \left(\frac{1}{\sqrt{2\pi\delta(E)^2}} \int_{26\,{\rm GeV}}^{m_\chi} d\bar{E} \frac{dN_\gamma(\bar{E})}{d\bar{E}} A_{\rm eff}(\bar{E}) e^{-\frac{(E-\bar{E})^2}{2\delta(E)^2}} \right) , \quad \text{(A.1)}$$

where $A_{\rm eff}$ is the effective area of the detector, $\delta(E)$ is the energy resolution, dN_γ/dE is the annihilation spectrum, and J is the J-factor for either the ON or OFF region. For $A_{\rm eff}$ and $\delta(E)$ we use the most up to date instrument response functions provided by the CTA Collaboration [70]. We take an observation time $t_{\rm obs} = 500$ h.

As is well known, the J-factor is defined by integration along the line of sight (l.o.s.) of the DM halo profile squared, $\rho^2(r)$:

$$J = \int_{\Delta\Omega} \int_{\rm l.o.s.} \rho^2[r(\theta)] dr(\theta) d\Omega \,, \quad \text{(A.2)}$$

where in the reference frame centred at the observer the distance from the GC depends on the azimuthal angle θ. Using the Einasto DM density profile [72], we obtain $J_{\rm ON}^{\rm Ein} = 7.44 \times 10^{21}\,{\rm GeV}^2/{\rm cm}^5$ and $J_{\rm OFF}^{\rm Ein} = 1.21 \times 10^{22}\,{\rm GeV}^2/{\rm cm}^5$ for the J-factors of the ON and OFF regions, respectively, in agreement with the results of [64]. The corresponding values for the NFW [73] profile are $J_{\rm ON}^{\rm NFW} = 3.89 \times 10^{21}\,{\rm GeV}^2/{\rm cm}^5$ and $J_{\rm OFF}^{\rm NFW} = 5.78 \times 10^{21}\,{\rm GeV}^2/{\rm cm}^5$.

To gauge the constraining power of the binned likelihood we compare the projected sensitivity for DM annihilating to $b\bar{b}$ for three different methods.

1. We first calculate the binned Poisson likelihood defined by

$$\mathcal{L} = \prod_{i,j} \frac{\mu_{ij}^{n_{ij}}}{n_{ij}!} e^{-\mu_{ij}} \,. \quad \text{(A.3)}$$

JHEP02(2015)014

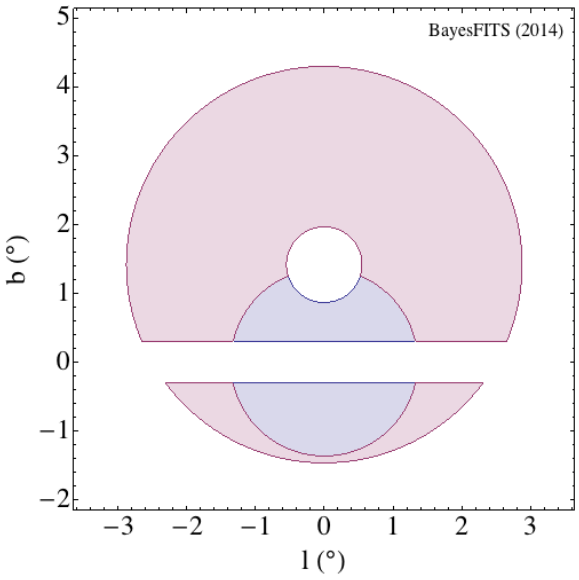

Figure 12. In blue, the **ON** region: the angular radius is $\Delta_{\rm cut} = 1.36°$. In pink, the **OFF** region: the offset from the GC is $b_{\rm off} = 1.42°$; the inner radius is $r_1 = 0.55°$ and the outer radius is $r_2 = 2.88°$. The strip of sky at $|b| < 0.3°$ is subtracted from the ON and OFF regions.

In eq. (A.3) μ_{ij} is the expected number of photons in bin ij, with the index i running over the energy bins and $j = 1, 2$ for the ON and OFF region, respectively. It is given by the sum of the background and the expected count from DM annihilation, eq. (A.1). n_{ij} is the number of photons counted in bin ij.

We find the 95% C.L. limit by setting n_{ij} equal to the number of background-only photons and calculating $\mathcal{L}$ by increasing the annihilation cross section from the best fit value ($\sigma v = 0$) until the difference in $-2\ln\mathcal{L}$ from the best fit value is 2.71 (one-sided 95% C.L.). We use an updated [70] background estimate provided by the CTA Collaboration [71].

2. In the limit of a single energy bin one can construct a test statistics for the background-only hypothesis [136]

$$-2\ln\mathcal{L} = 2\left[N_{\rm ON}\ln\left(\frac{1+\alpha}{\alpha}\frac{N_{\rm ON}}{N_{\rm ON}+N_{\rm OFF}}\right) + N_{\rm OFF}\ln\left((1+\alpha)\frac{N_{\rm OFF}}{N_{\rm ON}+N_{\rm OFF}}\right)\right], \tag{A.4}$$

where $N_{\rm ON}$ and $N_{\rm OFF}$ are the number of counts in the ON and OFF regions, respectively, and $\alpha = \Delta\Omega_{\rm ON}/\Delta\Omega_{\rm OFF}$ is the ratio of the ON and OFF solid angles. We calculate the projected sensitivity by setting $N_{\rm ON}$ and $N_{\rm OFF}$ equal to the expected number of counts $N_j = \sum_i \mu_{ij}$. We calculate $\alpha = 0.2457$. We will compare the sensitivity obtained with eq. (A.4), hereafter referred to as the Li and Ma method, with the binned likelihood method, eq. (A.3).

3. We finally compare the binned Poisson likelihood, eq. (A.3), to the binned Skellam distribution [137], on which the results of [63] are based. Note that the results of

JHEP02(2015)014

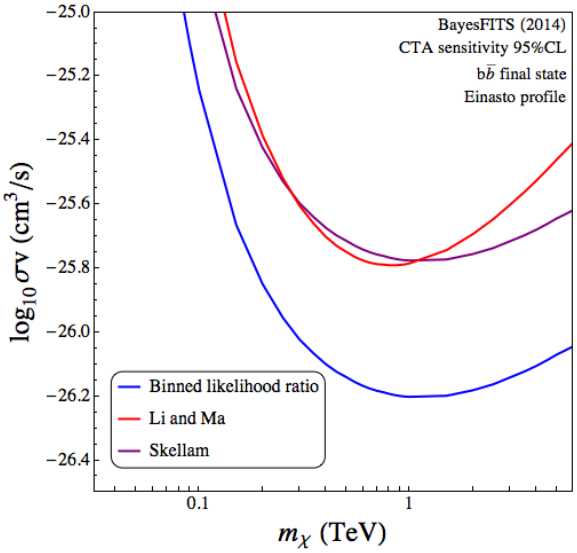

Figure 13. Comparison of the limits obtained using the three methods of calculating the likelihood for annihilation to the $b\bar{b}$ final state assuming the Einasto profile.

ref. [63] were used in our previous study [20] to estimate the sensitivity of CTA to the parameter space of the CMSSM and the NUHM.

If one calculates for each energy bin i the difference in the measured number of events $\theta_{\mathrm{diff},i} = n_{i,\mathrm{ON}} - \alpha\, n_{i,\mathrm{OFF}}$, the probability of observing a set of particular values $\{\theta_{\mathrm{diff},i}\}$ is given by the Skellam distribution

$$\mathcal{L}(\{\theta_{\mathrm{diff},i}\}) = \prod_i e^{-(N_{i,\mathrm{ON}}+\alpha N_{i,\mathrm{OFF}})} \left(\frac{N_{i,\mathrm{ON}}}{\alpha N_{i,\mathrm{OFF}}}\right)^{\frac{\theta_{\mathrm{diff},i}}{2}} I_{|\theta_{\mathrm{diff},i}|}(2\sqrt{\alpha N_{i,\mathrm{ON}} N_{i,\mathrm{OFF}}})\,, \tag{A.5}$$

where $N_{i,\mathrm{ON}} = \mu_{i1}$, $N_{i,\mathrm{OFF}} = \mu_{i2}$ are the expected numbers of photons and $I_{|\theta_{\mathrm{diff},i}|}$ is the $|\theta_{\mathrm{diff},i}|$th Bessel function of the first kind. The projected limit is obtained by setting $\theta_{\mathrm{diff},i} = 0$ for all the energy bins. One finds

$$\mathcal{L} = \prod_i e^{-(N_{i,\mathrm{ON}}+\alpha N_{i,\mathrm{OFF}})} I_0(2\sqrt{\alpha N_{i,\mathrm{ON}} N_{i,\mathrm{OFF}}})\,. \tag{A.6}$$

In figure 13 we show the limits obtained for the $b\bar{b}$ final state and Einasto profile using these three methods. For low masses the limits obtained using the Skellam distribution and the Li and Ma method are comparable. For larger masses the Li and Ma method loses sensitivity compared to the other two methods as they benefit from the data being binned by energy. The binned likelihood method produces the strongest limits and we adopt this method for producing our projected sensitivities. We find limits that are stronger than the estimates of [63] and [64] but comparable to [62].

It should be noted that we have not included uncertainties in the DM distribution, systematic uncertainties in the detector response, or included the diffuse γ-ray background.

JHEP02(2015)014

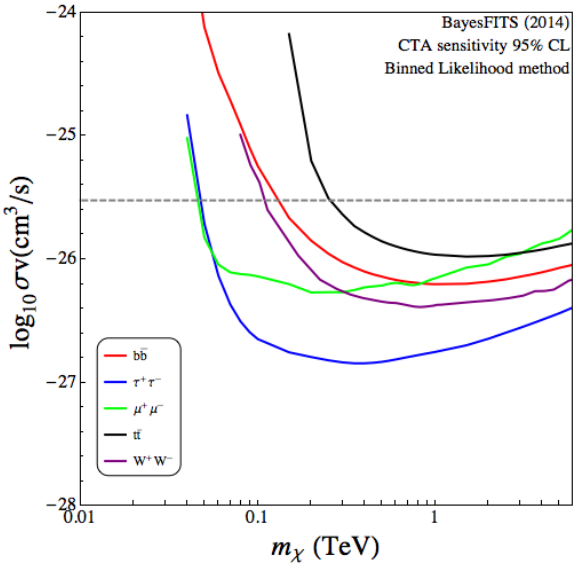

Figure 14. 95% C.L. CTA projected limits derived for the specific final states most commonly found in the pMSSM with the binned likelihood of eq. (A.3) for the Einasto profile. The limits for the W^+W^-, $b\bar{b}$, $t\bar{t}$, and $\tau^+\tau^-$ final states are compared to realistic MSSM models in figure 3.

The uncertainty in the DM distribution enters into the calculation of the limits through the J-factors in eq. (A.1). We account for this by presenting limits for two different realisations of the DM distribution, the NFW and Einasto profiles. We do not consider cored solutions [122, 123] for the halo profile, as they also require a reinterpretation of current limits regarding the wino. Nevertheless we comment on the impact of the Burkert [59] profile assumption on our plots in section 4.2.

The systematic uncertainty due to the finite energy resolution of the experiment already appears in eq. (A.1). However further systematic effects can be present such as varying acceptance across the field of view or uncertainties in the effective area.

Finally, the diffuse astrophysical γ-ray background around the galactic centre measured by H.E.S.S. [138] and Fermi-LAT [139] presents a challenge to this type of ON/OFF analysis since this background will be larger in the ON (signal) region than the OFF (background) region mimicking the searched for signal. Thus the sensitivity presented here is somewhat optimistic and would be reduced due to the diffuse background and systematic uncertainties, however the treatment of ref. [64] suggests that a morphological analysis could partially mitigate these effects.

Figure 14 shows the derived 95% C.L. limits for some specific final states including the most common primary annihilation channels found in the pMSSM using the binned likelihood of eq. (A.3). The limits obtained can probe values of σv below the "canonical" thermal relic value for all of the final states. We compare these to the actual final states found by the scan in figure 3, section 3.

JHEP02(2015)014

References

[1] M. Drees and G. Gerbier, *Mini-review of dark matter:* 2012, arXiv:1204.2373 [INSPIRE].

[2] PARTICLE DATA GROUP collaboration, K. Olive et al., *Review of particle physics*, *Chin. Phys.* **C38** (2014) 090001 [INSPIRE].

[3] J. Goodman et al., *Constraints on dark matter from colliders*, *Phys. Rev.* **D 82** (2010) 116010 [arXiv:1008.1783] [INSPIRE].

[4] P.J. Fox, R. Harnik, J. Kopp and Y. Tsai, *Missing energy signatures of dark matter at the LHC*, *Phys. Rev.* **D 85** (2012) 056011 [arXiv:1109.4398] [INSPIRE].

[5] XENON100 collaboration, E. Aprile et al., *Dark matter results from* 225 *live days of XENON*100 *data*, *Phys. Rev. Lett.* **109** (2012) 181301 [arXiv:1207.5988] [INSPIRE].

[6] LUX collaboration, D.S. Akerib et al., *First results from the LUX dark matter experiment at the Sanford Underground Research Facility*, *Phys. Rev. Lett.* **112** (2014) 091303 [arXiv:1310.8214] [INSPIRE].

[7] ATLAS collaboration, *Search for dark matter in events with a hadronically decaying W or Z boson and missing transverse momentum in pp collisions at* $\sqrt{s} = 8$ *TeV with the ATLAS detector*, *Phys. Rev. Lett.* **112** (2014) 041802 [arXiv:1309.4017] [INSPIRE].

[8] ATLAS collaboration, *Search for dark matter in events with a Z boson and missing transverse momentum in pp collisions at* $\sqrt{s} = 8$ *TeV with the ATLAS detector*, *Phys. Rev.* **D 90** (2014) 012004 [arXiv:1404.0051] [INSPIRE].

[9] CMS collaboration, *Search for dark matter, extra dimensions and unparticles in monojet events in proton-proton collisions at* $\sqrt{s} = 8$ *TeV*, arXiv:1408.3583 [INSPIRE].

[10] CMS collaboration, *Monophoton search*, CMS-PAS-EXO-12-047, CERN, Geneva Switzerland (2012).

[11] FERMI-LAT collaboration, M. Ackermann et al., *Dark matter constraints from observations of* 25 *Milky Way satellite galaxies with the Fermi Large Area Telescope*, *Phys. Rev.* **D 89** (2014) 042001 [arXiv:1310.0828] [INSPIRE].

[12] H.E.S.S. collaboration, A. Abramowski et al., *Search for a dark matter annihilation signal from the galactic center halo with H.E.S.S.*, *Phys. Rev. Lett.* **106** (2011) 161301 [arXiv:1103.3266] [INSPIRE].

[13] ICECUBE collaboration, R. Abbasi et al., *Multi-year search for dark matter annihilations in the sun with the AMANDA-II and IceCube detectors*, *Phys. Rev.* **D 85** (2012) 042002 [arXiv:1112.1840] [INSPIRE].

[14] ICECUBE collaboration, M.G. Aartsen et al., *Search for dark matter annihilations in the sun with the* 79*-string IceCube detector*, *Phys. Rev. Lett.* **110** (2013) 131302 [arXiv:1212.4097] [INSPIRE].

[15] ANTARES collaboration, S. Adrian-Martinez et al., *First results on dark matter annihilation in the sun using the ANTARES neutrino telescope*, *JCAP* **11** (2013) 032 [arXiv:1302.6516] [INSPIRE].

[16] K.L. Chan, U. Chattopadhyay and P. Nath, *Naturalness, weak scale supersymmetry and the prospect for the observation of supersymmetry at the Tevatron and at the CERN LHC*, *Phys. Rev.* **D 58** (1998) 096004 [hep-ph/9710473] [INSPIRE].

JHEP02(2015)014

[17] J.L. Feng, K.T. Matchev and T. Moroi, *Multi-TeV scalars are natural in minimal supergravity*, *Phys. Rev. Lett.* **84** (2000) 2322 [hep-ph/9908309] [INSPIRE].

[18] J.L. Feng, K.T. Matchev and T. Moroi, *Focus points and naturalness in supersymmetry*, *Phys. Rev.* **D 61** (2000) 075005 [hep-ph/9909334] [INSPIRE].

[19] A. Fowlie, K. Kowalska, L. Roszkowski, E.M. Sessolo and Y.-L.S. Tsai, *Dark matter and collider signatures of the MSSM*, *Phys. Rev.* **D 88** (2013) 055012 [arXiv:1306.1567] [INSPIRE].

[20] L. Roszkowski, E.M. Sessolo and A.J. Williams, *What next for the CMSSM and the NUHM: improved prospects for superpartner and dark matter detection*, *JHEP* **08** (2014) 067 [arXiv:1405.4289] [INSPIRE].

[21] L. Calibbi, J.M. Lindert, T. Ota and Y. Takanishi, *Cornering light neutralino dark matter at the LHC*, *JHEP* **10** (2013) 132 [arXiv:1307.4119] [INSPIRE].

[22] L. Calibbi, J.M. Lindert, T. Ota and Y. Takanishi, *LHC tests of light neutralino dark matter without light sfermions*, *JHEP* **11** (2014) 106 [arXiv:1410.5730] [INSPIRE].

[23] A. Arbey, M. Battaglia and F. Mahmoudi, *Combining monojet, supersymmetry and dark matter searches*, *Phys. Rev.* **D 89** (2014) 077701 [arXiv:1311.7641] [INSPIRE].

[24] M. Chakraborti, U. Chattopadhyay, A. Choudhury, A. Datta and S. Poddar, *The electroweak sector of the pMSSM in the light of LHC — 8 TeV and other data*, *JHEP* **07** (2014) 019 [arXiv:1404.4841] [INSPIRE].

[25] ATLAS collaboration, *Search for direct production of charginos, neutralinos and sleptons in final states with two leptons and missing transverse momentum in pp collisions at* $\sqrt{s} = 8$ *TeV with the ATLAS detector*, *JHEP* **05** (2014) 071 [arXiv:1403.5294] [INSPIRE].

[26] ATLAS collaboration, *Search for direct production of charginos and neutralinos in events with three leptons and missing transverse momentum in* $\sqrt{s} = 8$ *TeV pp collisions with the ATLAS detector*, *JHEP* **04** (2014) 169 [arXiv:1402.7029] [INSPIRE].

[27] CMS collaboration, *Searches for electroweak production of charginos, neutralinos and sleptons decaying to leptons and W, Z and Higgs bosons in pp collisions at* 8 *TeV*, *Eur. Phys. J.* **C 74** (2014) 3036 [arXiv:1405.7570] [INSPIRE].

[28] CMS collaboration, *Searches for electroweak neutralino and chargino production in channels with Higgs, Z and W bosons in pp collisions at* 8 *TeV*, *Phys. Rev.* **D 90** (2014) 092007 [arXiv:1409.3168] [INSPIRE].

[29] C. Strege et al., *Global fits of the CMSSM and NUHM including the LHC Higgs discovery and new XENON*100 *constraints*, *JCAP* **04** (2013) 013 [arXiv:1212.2636] [INSPIRE].

[30] M.E. Cabrera, J.A. Casas and R.R. de Austri, *The health of SUSY after the Higgs discovery and the XENON*100 *data*, *JHEP* **07** (2013) 182 [arXiv:1212.4821] [INSPIRE].

[31] K. Kowalska, L. Roszkowski and E.M. Sessolo, *Two ultimate tests of constrained supersymmetry*, *JHEP* **06** (2013) 078 [arXiv:1302.5956] [INSPIRE].

[32] O. Buchmueller et al., *The CMSSM and NUHM*1 *after LHC run* 1, *Eur. Phys. J.* **C 74** (2014) 2922 [arXiv:1312.5250] [INSPIRE].

[33] O. Buchmueller et al., *The NUHM*2 *after LHC run* 1, *Eur. Phys. J.* **C 74** (2014) 3212 [arXiv:1408.4060] [INSPIRE].

[34] P. Bechtle et al., *How alive is constrained SUSY really?*, arXiv:1410.6035 [INSPIRE].

JHEP02(2015)014

[35] G.L. Kane, C.F. Kolda, L. Roszkowski and J.D. Wells, *Study of constrained minimal supersymmetry*, *Phys. Rev.* **D 49** (1994) 6173 [hep-ph/9312272] [INSPIRE].

[36] ATLAS collaboration, *Observation of a new particle in the search for the standard model Higgs boson with the ATLAS detector at the LHC*, *Phys. Lett.* **B 716** (2012) 1 [arXiv:1207.7214] [INSPIRE].

[37] CMS collaboration, *Observation of a new boson at a mass of* 125 *GeV with the CMS experiment at the LHC*, *Phys. Lett.* **B 716** (2012) 30 [arXiv:1207.7235] [INSPIRE].

[38] S. Profumo and C.E. Yaguna, *A statistical analysis of supersymmetric dark matter in the MSSM after WMAP*, *Phys. Rev.* **D 70** (2004) 095004 [hep-ph/0407036] [INSPIRE].

[39] N. Arkani-Hamed, A. Delgado and G.F. Giudice, *The well-tempered neutralino*, *Nucl. Phys.* **B 741** (2006) 108 [hep-ph/0601041] [INSPIRE].

[40] L. Roszkowski, R. Ruiz de Austri, R. Trotta, Y.-L.S. Tsai and T.A. Varley, *Global fits of the non-universal Higgs model*, *Phys. Rev.* **D 83** (2011) 015014 [arXiv:0903.1279] [INSPIRE].

[41] A. Kaminska, G.G. Ross and K. Schmidt-Hoberg, *Non-universal gaugino masses and fine tuning implications for SUSY searches in the MSSM and the GNMSSM*, *JHEP* **11** (2013) 209 [arXiv:1308.4168] [INSPIRE].

[42] K. Kowalska, L. Roszkowski, E.M. Sessolo and S. Trojanowski, *Low fine tuning in the MSSM with higgsino dark matter and unification constraints*, *JHEP* **04** (2014) 166 [arXiv:1402.1328] [INSPIRE].

[43] M. Chakraborti, U. Chattopadhyay, S. Rao and D.P. Roy, *Higgsino dark matter in nonuniversal gaugino mass models*, arXiv:1411.4517 [INSPIRE].

[44] G.F. Giudice, M.A. Luty, H. Murayama and R. Rattazzi, *Gaugino mass without singlets*, *JHEP* **12** (1998) 027 [hep-ph/9810442] [INSPIRE].

[45] L. Randall and R. Sundrum, *Out of this world supersymmetry breaking*, *Nucl. Phys.* **B 557** (1999) 79 [hep-th/9810155] [INSPIRE].

[46] L.J. Hall and Y. Nomura, *Spread supersymmetry*, *JHEP* **01** (2012) 082 [arXiv:1111.4519] [INSPIRE].

[47] A. Arvanitaki, N. Craig, S. Dimopoulos and G. Villadoro, *Mini-split*, *JHEP* **02** (2013) 126 [arXiv:1210.0555] [INSPIRE].

[48] L.J. Hall, Y. Nomura and S. Shirai, *Spread supersymmetry with wino LSP: gluino and dark matter signals*, *JHEP* **01** (2013) 036 [arXiv:1210.2395] [INSPIRE].

[49] N. Arkani-Hamed, A. Gupta, D.E. Kaplan, N. Weiner and T. Zorawski, *Simply unnatural supersymmetry*, arXiv:1212.6971 [INSPIRE].

[50] T. Cohen, M. Lisanti, A. Pierce and T.R. Slatyer, *Wino dark matter under siege*, *JCAP* **10** (2013) 061 [arXiv:1307.4082] [INSPIRE].

[51] J. Fan and M. Reece, *In wino veritas? Indirect searches shed light on neutralino dark matter*, *JHEP* **10** (2013) 124 [arXiv:1307.4400] [INSPIRE].

[52] A. Hryczuk, I. Cholis, R. Iengo, M. Tavakoli and P. Ullio, *Indirect detection analysis: wino dark matter case study*, *JCAP* **07** (2014) 031 [arXiv:1401.6212] [INSPIRE].

[53] J. Hisano, S. Matsumoto and M.M. Nojiri, *Unitarity and higher order corrections in neutralino dark matter annihilation into two photons*, *Phys. Rev.* **D 67** (2003) 075014 [hep-ph/0212022] [INSPIRE].

JHEP02(2015)014

[54] J. Hisano, S. Matsumoto, M.M. Nojiri and O. Saito, *Non-perturbative effect on dark matter annihilation and gamma ray signature from galactic center*, *Phys. Rev.* **D 71** (2005) 063528 [hep-ph/0412403] [INSPIRE].

[55] J. Hisano, S. Matsumoto, M. Nagai, O. Saito and M. Senami, *Non-perturbative effect on thermal relic abundance of dark matter*, *Phys. Lett.* **B 646** (2007) 34 [hep-ph/0610249] [INSPIRE].

[56] M. Cirelli, A. Strumia and M. Tamburini, *Cosmology and astrophysics of minimal dark matter*, *Nucl. Phys.* **B 787** (2007) 152 [arXiv:0706.4071] [INSPIRE].

[57] A. Hryczuk, R. Iengo and P. Ullio, *Relic densities including Sommerfeld enhancements in the MSSM*, *JHEP* **03** (2011) 069 [arXiv:1010.2172] [INSPIRE].

[58] H.E.S.S. collaboration, A. Abramowski et al., *Search for photon-linelike signatures from dark matter annihilations with H.E.S.S.*, *Phys. Rev. Lett.* **110** (2013) 041301 [arXiv:1301.1173] [INSPIRE].

[59] A. Burkert, *The structure of dark matter halos in dwarf galaxies*, *IAU Symp.* **171** (1996) 175 [*Astrophys. J.* **447** (1995) L25] [astro-ph/9504041] [INSPIRE].

[60] B.S. Acharya et al., *Introducing the CTA concept*, *Astropart. Phys.* **43** (2013) 3 [INSPIRE].

[61] CTA collaboration, M. Doro et al., *Dark matter and fundamental physics with the Cherenkov Telescope Array*, *Astropart. Phys.* **43** (2013) 189 [arXiv:1208.5356] [INSPIRE].

[62] M. Wood et al., *Prospects for indirect detection of dark matter with CTA*, arXiv:1305.0302 [INSPIRE].

[63] M. Pierre, J.M. Siegal-Gaskins and P. Scott, *Sensitivity of CTA to dark matter signals from the galactic center*, *JCAP* **06** (2014) 024 [arXiv:1401.7330] [INSPIRE].

[64] H. Silverwood, C. Weniger, P. Scott and G. Bertone, *A realistic assessment of the CTA sensitivity to dark matter annihilation*, arXiv:1408.4131 [INSPIRE].

[65] K.N. Abazajian and J.P. Harding, *Constraints on WIMP and Sommerfeld-enhanced dark matter annihilation from H.E.S.S. observations of the galactic center*, *JCAP* **01** (2012) 041 [arXiv:1110.6151] [INSPIRE].

[66] J. Aleksić et al., *Optimized dark matter searches in deep observations of Segue* 1 *with MAGIC*, *JCAP* **02** (2014) 008 [arXiv:1312.1535] [INSPIRE].

[67] VERITAS collaboration, A. Geringer-Sameth, *The VERITAS dark matter program*, arXiv:1303.1406 [INSPIRE].

[68] MSSM Working Group collaboration, A. Djouadi et al., *The minimal supersymmetric standard model: group summary report*, hep-ph/9901246 [INSPIRE].

[69] M. Cahill-Rowley et al., *Complementarity of dark matter searches in the pMSSM*, arXiv:1405.6716 [INSPIRE].

[70] J. Carr, private communication.

[71] K. Bernlöhr et al., *Monte Carlo design studies for the Cherenkov Telescope Array*, *Astropart. Phys.* **43** (2013) 171 [arXiv:1210.3503] [INSPIRE].

[72] J. Einasto, *On the construction of a composite model for the galaxy and on the determination of the system of galactic parameters*, *Trudy Astrofiz. Inst. Alma-Ata* **5** (1965) 87.

JHEP02(2015)014

[73] J.F. Navarro, C.S. Frenk and S.D.M. White, *The structure of cold dark matter halos*, *Astrophys. J.* **462** (1996) 563 [astro-ph/9508025] [INSPIRE].

[74] ATLAS, CDF, CMS and D0 collaborations, *First combination of Tevatron and LHC measurements of the top-quark mass*, arXiv:1403.4427 [INSPIRE].

[75] A. Fowlie et al., *The CMSSM favoring new territories: the impact of new LHC limits and a 125 GeV Higgs*, *Phys. Rev.* **D 86** (2012) 075010 [arXiv:1206.0264] [INSPIRE].

[76] K. Kowalska et al., *Constrained next-to-minimal supersymmetric standard model with a 126 GeV Higgs boson: a global analysis*, *Phys. Rev.* **D 87** (2013) 115010 [arXiv:1211.1693] [INSPIRE].

[77] F. Feroz, M.P. Hobson and M. Bridges, *MultiNest: an efficient and robust Bayesian inference tool for cosmology and particle physics*, *Mon. Not. Roy. Astron. Soc.* **398** (2009) 1601 [arXiv:0809.3437] [INSPIRE].

[78] B.C. Allanach, *SOFTSUSY: a program for calculating supersymmetric spectra*, *Comput. Phys. Commun.* **143** (2002) 305 [hep-ph/0104145] [INSPIRE].

[79] S. Heinemeyer, W. Hollik and G. Weiglein, *FeynHiggs: a program for the calculation of the masses of the neutral CP even Higgs bosons in the MSSM*, *Comput. Phys. Commun.* **124** (2000) 76 [hep-ph/9812320] [INSPIRE].

[80] S. Heinemeyer, W. Hollik and G. Weiglein, *The masses of the neutral CP-even Higgs bosons in the MSSM: accurate analysis at the two loop level*, *Eur. Phys. J.* **C 9** (1999) 343 [hep-ph/9812472] [INSPIRE].

[81] G. Degrassi, S. Heinemeyer, W. Hollik, P. Slavich and G. Weiglein, *Towards high precision predictions for the MSSM Higgs sector*, *Eur. Phys. J.* **C 28** (2003) 133 [hep-ph/0212020] [INSPIRE].

[82] M. Frank et al., *The Higgs boson masses and mixings of the complex MSSM in the Feynman-diagrammatic approach*, *JHEP* **02** (2007) 047 [hep-ph/0611326] [INSPIRE].

[83] T. Hahn, S. Heinemeyer, W. Hollik, H. Rzehak and G. Weiglein, *High-precision predictions for the light CP-even Higgs boson mass of the minimal supersymmetric standard model*, *Phys. Rev. Lett.* **112** (2014) 141801 [arXiv:1312.4937] [INSPIRE].

[84] P. Bechtle, S. Heinemeyer, O. Stål, T. Stefaniak and G. Weiglein, *HiggsSignals: confronting arbitrary Higgs sectors with measurements at the Tevatron and the LHC*, *Eur. Phys. J.* **C 74** (2014) 2711 [arXiv:1305.1933] [INSPIRE].

[85] P. Bechtle, O. Brein, S. Heinemeyer, G. Weiglein and K.E. Williams, *HiggsBounds: confronting arbitrary Higgs sectors with exclusion bounds from LEP and the Tevatron*, *Comput. Phys. Commun.* **181** (2010) 138 [arXiv:0811.4169] [INSPIRE].

[86] P. Bechtle, O. Brein, S. Heinemeyer, G. Weiglein and K.E. Williams, *HiggsBounds* 2.0.0*: confronting neutral and charged Higgs sector predictions with exclusion bounds from LEP and the Tevatron*, *Comput. Phys. Commun.* **182** (2011) 2605 [arXiv:1102.1898] [INSPIRE].

[87] P. Bechtle et al., *HiggsBounds-4: improved tests of extended Higgs sectors against exclusion bounds from LEP, the Tevatron and the LHC*, *Eur. Phys. J.* **C 74** (2014) 2693 [arXiv:1311.0055] [INSPIRE].

[88] F. Mahmoudi, *SuperIso v2.3: a program for calculating flavor physics observables in supersymmetry*, *Comput. Phys. Commun.* **180** (2009) 1579 [arXiv:0808.3144] [INSPIRE].

JHEP02(2015)014

[89] G. Bélanger, F. Boudjema, A. Pukhov and A. Semenov, *MicrOMEGAs$_3$: a program for calculating dark matter observables*, *Comput. Phys. Commun.* **185** (2014) 960 [arXiv:1305.0237] [INSPIRE].

[90] K. Cheung, Y.-L.S. Tsai, P.-Y. Tseng, T.-C. Yuan and A. Zee, *Global study of the simplest scalar phantom dark matter model*, *JCAP* **10** (2012) 042 [arXiv:1207.4930] [INSPIRE].

[91] PLANCK collaboration, P.A.R. Ade et al., *Planck* 2013 *results. XVI. Cosmological parameters*, *Astron. Astrophys.* **571** (2014) A16 [arXiv:1303.5076] [INSPIRE].

[92] PARTICLE DATA GROUP collaboration, J. Beringer et al., *Review of particle physics (RPP)*, *Phys. Rev.* **D 86** (2012) 010001 [INSPIRE].

[93] *Electroweak radiative B decays webpage*, http://www.slac.stanford.edu/xorg/hfag/rare/2012/radll/index.html.

[94] BELLE collaboration, I. Adachi et al., *Evidence for $B^- \to \tau^- \bar{\nu}_\tau$ with a hadronic tagging method using the full data sample of Belle*, *Phys. Rev. Lett.* **110** (2013) 131801 [arXiv:1208.4678] [INSPIRE].

[95] LHCb collaboration, *Measurement of the $B_s^0 \to \mu^+\mu^-$ branching fraction and search for $B^0 \to \mu^+\mu^-$ decays at the LHCb experiment*, *Phys. Rev. Lett.* **111** (2013) 101805 [arXiv:1307.5024] [INSPIRE].

[96] CMS collaboration, *Measurement of the $B_s \to \mu^+\mu^-$ branching fraction and search for $B^0 \to \mu^+\mu^-$ with the CMS experiment*, *Phys. Rev. Lett.* **111** (2013) 101804 [arXiv:1307.5025] [INSPIRE].

[97] K. Kowalska and E.M. Sessolo, *Natural MSSM after the LHC* 8 *TeV run*, *Phys. Rev.* **D 88** (2013) 075001 [arXiv:1307.5790] [INSPIRE].

[98] MUON G-2 collaboration, G.W. Bennett et al., *Final report of the muon E*821 *anomalous magnetic moment measurement at BNL*, *Phys. Rev.* **D 73** (2006) 072003 [hep-ex/0602035] [INSPIRE].

[99] J.P. Miller, E. de Rafael and B.L. Roberts, *Muon (g-2): experiment and theory*, *Rept. Prog. Phys.* **70** (2007) 795 [hep-ph/0703049] [INSPIRE].

[100] J.R. Ellis, L. Roszkowski and Z. Lalak, *Higgs effects on the relic supersymmetric particle density*, *Phys. Lett.* **B 245** (1990) 545 [INSPIRE].

[101] B. Cabrera, L.M. Krauss and F. Wilczek, *Bolometric detection of neutrinos*, *Phys. Rev. Lett.* **55** (1985) 25 [INSPIRE].

[102] J. Monroe and P. Fisher, *Neutrino backgrounds to dark matter searches*, *Phys. Rev.* **D 76** (2007) 033007 [arXiv:0706.3019] [INSPIRE].

[103] J. Billard, L. Strigari and E. Figueroa-Feliciano, *Implication of neutrino backgrounds on the reach of next generation dark matter direct detection experiments*, *Phys. Rev.* **D 89** (2014) 023524 [arXiv:1307.5458] [INSPIRE].

[104] K. Griest, M. Kamionkowski and M.S. Turner, *Supersymmetric dark matter above the W mass*, *Phys. Rev.* **D 41** (1990) 3565 [INSPIRE].

[105] M. Drees and M.M. Nojiri, *The neutralino relic density in minimal $N = 1$ supergravity*, *Phys. Rev.* **D 47** (1993) 376 [hep-ph/9207234] [INSPIRE].

JHEP02(2015)014

[106] J.R. Ellis, T. Falk and K.A. Olive, *Neutralino-stau coannihilation and the cosmological upper limit on the mass of the lightest supersymmetric particle*, *Phys. Lett.* **B 444** (1998) 367 [hep-ph/9810360] [INSPIRE].

[107] J.R. Ellis, A. Ferstl and K.A. Olive, *Reevaluation of the elastic scattering of supersymmetric dark matter*, *Phys. Lett.* **B 481** (2000) 304 [hep-ph/0001005] [INSPIRE].

[108] J.R. Ellis, A. Ferstl and K.A. Olive, *Exploration of elastic scattering rates for supersymmetric dark matter*, *Phys. Rev.* **D 63** (2001) 065016 [hep-ph/0007113] [INSPIRE].

[109] J.R. Ellis, K.A. Olive, Y. Santoso and V.C. Spanos, *Update on the direct detection of supersymmetric dark matter*, *Phys. Rev.* **D 71** (2005) 095007 [hep-ph/0502001] [INSPIRE].

[110] H. Baer, A. Mustafayev, E.-K. Park and X. Tata, *Target dark matter detection rates in models with a well-tempered neutralino*, *JCAP* **01** (2007) 017 [hep-ph/0611387] [INSPIRE].

[111] P. Huang and C.E.M. Wagner, *Blind spots for neutralino dark matter in the MSSM with an intermediate m_A*, *Phys. Rev.* **D 90** (2014) 015018 [arXiv:1404.0392] [INSPIRE].

[112] J. Edsjo and P. Gondolo, *Neutralino relic density including coannihilations*, *Phys. Rev.* **D 56** (1997) 1879 [hep-ph/9704361] [INSPIRE].

[113] A. Hryczuk and R. Iengo, *The one-loop and Sommerfeld electroweak corrections to the wino dark matter annihilation*, *JHEP* **01** (2012) 163 [*Erratum ibid.* **06** (2012) 137] [arXiv:1111.2916] [INSPIRE].

[114] L.J. Hall, K. Jedamzik, J. March-Russell and S.M. West, *Freeze-in production of FIMP dark matter*, *JHEP* **03** (2010) 080 [arXiv:0911.1120] [INSPIRE].

[115] A.J. Williams, C. Boehm, S.M. West and D.A. Vasquez, *Regenerating WIMPs in the light of direct and indirect detection*, *Phys. Rev.* **D 86** (2012) 055018 [arXiv:1204.3727] [INSPIRE].

[116] G. Jungman, M. Kamionkowski and K. Griest, *Supersymmetric dark matter*, *Phys. Rept.* **267** (1996) 195 [hep-ph/9506380] [INSPIRE].

[117] PAMELA collaboration, O. Adriani et al., *An anomalous positron abundance in cosmic rays with energies* 1.5–100 *GeV*, *Nature* **458** (2009) 607 [arXiv:0810.4995] [INSPIRE].

[118] AMS collaboration, M. Aguilar et al., *First result from the alpha magnetic spectrometer on the international space station: precision measurement of the positron fraction in primary cosmic rays of* 0.5–350 *GeV*, *Phys. Rev. Lett.* **110** (2013) 141102 [INSPIRE].

[119] M. Bauer, T. Cohen, R.J. Hill and M.P. Solon, *Soft collinear effective theory for heavy WIMP annihilation*, arXiv:1409.7392 [INSPIRE].

[120] E.A. Baltz and J. Edsjo, *Positron propagation and fluxes from neutralino annihilation in the halo*, *Phys. Rev.* **D 59** (1998) 023511 [astro-ph/9808243] [INSPIRE].

[121] I.V. Moskalenko and A.W. Strong, *Production and propagation of cosmic ray positrons and electrons*, *Astrophys. J.* **493** (1998) 694 [astro-ph/9710124] [INSPIRE].

[122] P. Salucci et al., *The universal rotation curve of spiral galaxies. 2. The dark matter distribution out to the virial radius*, *Mon. Not. Roy. Astron. Soc.* **378** (2007) 41 [astro-ph/0703115] [INSPIRE].

[123] F. Nesti and P. Salucci, *The dark matter halo of the Milky Way, AD* 2013, *JCAP* **07** (2013) 016 [arXiv:1304.5127] [INSPIRE].

[124] V. Bertin for the ANTARES Dark Matter Group, private communication.

JHEP02(2015)014

[125] XENON1T collaboration, E. Aprile, *The XENON1T dark matter search experiment*, *Springer Proc. Phys.* **148** (2013) 93 [arXiv:1206.6288] [INSPIRE].

[126] P.A. Amaudruz et al., *DEAP-3600 dark matter search*, arXiv:1410.7673 [INSPIRE].

[127] D.C. Malling et al., *After LUX: the LZ program*, arXiv:1110.0103 [INSPIRE].

[128] V. Barger, J. Kumar, D. Marfatia and E.M. Sessolo, *Fermion WIMPless dark matter at DeepCore and IceCube*, *Phys. Rev.* **D 81** (2010) 115010 [arXiv:1004.4573] [INSPIRE].

[129] L. Roszkowski, E.M. Sessolo and Y.-L.S. Tsai, *Bayesian implications of current LHC supersymmetry and dark matter detection searches for the constrained MSSM*, *Phys. Rev.* **D 86** (2012) 095005 [arXiv:1202.1503] [INSPIRE].

[130] M.C. Gonzalez-Garcia, F. Halzen and S. Mohapatra, *Identifying galactic PeVatrons with neutrinos*, *Astropart. Phys.* **31** (2009) 437 [arXiv:0902.1176] [INSPIRE].

[131] V. Barger, Y. Gao and D. Marfatia, *Dark matter at DeepCore and IceCube*, *Phys. Rev.* **D 83** (2011) 055012 [arXiv:1101.4410] [INSPIRE].

[132] ATLAS collaboration, *Search for strong production of supersymmetric particles in final states with missing transverse momentum and at least three b-jets at* $\sqrt{s} = 8$ *TeV proton-proton collisions with the ATLAS detector*, *JHEP* **10** (2014) 024 [arXiv:1407.0600] [INSPIRE].

[133] ATLAS collaboration, *Search for top squark pair production in final states with one isolated lepton, jets and missing transverse momentum in* $\sqrt{s} = 8$ *TeV pp collisions with the ATLAS detector*, *JHEP* **11** (2014) 118 [arXiv:1407.0583] [INSPIRE].

[134] ATLAS collaboration, *Search for direct third-generation squark pair production in final states with missing transverse momentum and two b-jets in* $\sqrt{s} = 8$ *TeV pp collisions with the ATLAS detector*, *JHEP* **10** (2013) 189 [arXiv:1308.2631] [INSPIRE].

[135] CMS collaboration, *Search for supersymmetry in pp collisions at* $\sqrt{s} = 8$ *TeV in events with a single lepton, large jet multiplicity and multiple b jets*, *Phys. Lett.* **B 733** (2014) 328 [arXiv:1311.4937] [INSPIRE].

[136] T.-P. Li and Y.-Q. Ma, *Analysis methods for results in gamma-ray astronomy*, *Astrophys. J.* **272** (1983) 317 [INSPIRE].

[137] J.G. Skellam, *The frequency distribution of the difference between two Poisson variates belonging to different populations*, *J. Roy. Statist. Soc.* **109** (1946) 296.

[138] H.E.S.S. collaboration, F. Aharonian et al., *Discovery of very-high-energy gamma-rays from the galactic centre ridge*, *Nature* **439** (2006) 695 [astro-ph/0603021] [INSPIRE].

[139] FERMI-LAT collaboration, *Fermi-LAT observations of the diffuse gamma-ray emission: implications for cosmic rays and the interstellar medium*, *Astrophys. J.* **750** (2012) 3 [arXiv:1202.4039] [INSPIRE].

JHEP02(2015)014